

Statistical mechanics of continual learning: variational principle and mean-field potential

Chan Li^{1,*} Zhenye Huang^{2,*} Wenxuan Zou^{1,*} and Haiping Huang^{1†}

¹*PMI Lab, School of Physics, Sun Yat-sen University,
Guangzhou 510275, People's Republic of China and*

²*CAS Key Laboratory for Theoretical Physics,
Institute of Theoretical Physics, Chinese Academy of Sciences,
Beijing 100190, People's Republic of China*

(Dated: June 21, 2023)

arXiv:2212.02846v4 [cond-mat.stat-mech] 20 Jun 2023

Abstract

An obstacle to artificial general intelligence is set by continual learning of multiple tasks of different nature. Recently, various heuristic tricks, both from machine learning and from neuroscience angles, were proposed, but they lack a unified theory ground. Here, we focus on continual learning in single-layered and multi-layered neural networks of binary weights. A variational Bayesian learning setting is thus proposed, where the neural networks are trained in a field-space, rather than gradient-ill-defined discrete-weight space, and furthermore, weight uncertainty is naturally incorporated, and modulates synaptic resources among tasks. From a physics perspective, we translate the variational continual learning into Franz-Parisi thermodynamic potential framework, where previous task knowledge acts as a prior and a reference as well. We thus interpret the continual learning of the binary perceptron in a teacher-student setting as a Franz-Parisi potential computation. The learning performance can then be analytically studied with mean-field order parameters, whose predictions coincide with numerical experiments using stochastic gradient descent methods. Based on the variational principle and Gaussian field approximation of internal preactivations in hidden layers, we also derive the learning algorithm considering weight uncertainty, which solves the continual learning with binary weights using multi-layered neural networks, and performs better than the currently available metaplasticity algorithm where binary synapses bear hidden continuous states and the synaptic plasticity is modulated by a heuristic regularization function. Our proposed principled frameworks also connect to elastic weight consolidation, weight-uncertainty modulated learning, and neuroscience inspired metaplasticity, providing a theory-grounded method for the real-world multi-task learning with deep networks.

*Equal contribution.

†Electronic address: huanghp7@mail.sysu.edu.cn

I. INTRODUCTION

The environment an intelligent agent faces is commonly highly structured, and moreover, multiple tasks encoding this structure occur in sequence. Therefore, it is important for the agent to learn the continually evolving structures embedded in sequential tasks, i.e., transfer the knowledge gained from previous experiences to the learning of a current novel or unfamiliar task. However, during this continual learning, it is well-known that the previous task knowledge may be erased after learning a new task (so-called catastrophic forgetting [1, 2]). Uncovering neural mechanisms underlying a successful continual learning especially in the natural world presents a challenge in the current AI and even neuroscience research. There also emerge recently interesting works on biological neuronal networks in this regard [3–5], and the neuroscience research provides in turn insights for improving the performance of continual learning in artificial neural networks [6–8].

To avoid catastrophic forgetting, the machine learning community also proposed many heuristic strategies. For example, the elastic weight consolidation method introduces the Fisher information matrix to measure weight importance in the consecutive task learning [9], which is further improved by tracking individual weight contribution over the entire dynamics of training loss [10]. An attention mask can also be learned to alleviate the catastrophic forgetting [11]. Another important line is using the Bayesian approach [12]. This line shows that the synaptic uncertainty plays a significant role in taking the learning trade-off between two consecutive tasks [13–16]. We remark that these heuristic strategies have diverse design principles, but from a statistical physics perspective, they can be put under a unified framework of variational mean-field theory. Although recent theoretical works focused on phase transitions in transfer learning from source task to target task [17] and on-line learning dynamics of teacher-student setup [18–20], these works did not take into account weight uncertainty, which is an essential factor in learning neural networks [21], including more efficient and robust binary-weight networks. In addition, a recent study pointed out that the concept of meta-plasticity from brain science plays a key role in the continual learning of binary-weight neural networks [8]. This concept highlights that the binary synapse bears a hidden continuous state, and the synaptic plasticity is modulated by a heuristic regularization function. Our theoretical framework demonstrates that a variational principle can be constructed to explain the role of synaptic uncertainty, and moreover, the knowledge-

transfer between tasks can be actually captured by a thermodynamic potential [22], from which the learning performance can be predicted.

In this work, we not only carry out a thorough theoretical analysis of a toy teacher-student learning setting, where both tasks of a certain level of similarity are learned in sequence, but also apply the same principle to deep continual learning of structured datasets, which demonstrates the effectiveness of the variational mean-field principle, especially in the binary-weight neural networks where only meta-plasticity was previously proposed. Overall, our theory bridges statistical physics, especially the concept of the Franz-Parisi potential, originally studied in mean-field spin glass models [23], to theoretical underpinnings of the challenging continual learning. This connection may prove fruitful in future researches.

II. CONTINUAL LEARNING WITH BINARY PERCEPTRON

The binary perceptron offers an ideal candidate for understanding non-convex learning, as a theoretical analysis is possible by using statistical physics methods [24]. Here, we will use a teacher-student setting to perform the theoretical analysis of variational continual learning, in which the ground truth network is quenched before learning. In this section of toy model analysis, we use $\boldsymbol{\xi}$ and \boldsymbol{W} to indicate the student's and teacher's weights, respectively. In the next section of training deep networks (no ground truth in this case), we use \boldsymbol{w} to indicate the weights to learn.

A. Learning setting

The standard perceptron is a single-layered network with N binary input nodes, $x_i = \pm 1$ ($i = 1, 2, \dots, N$), and a single binary output node, $y = \pm 1$, which is connected by N binary weights $\xi_i = \pm 1$ ($i = 1, 2, \dots, N$). Given an input \boldsymbol{x} , the output is specified by $y = \text{sign}(\frac{1}{\sqrt{N}} \sum_i x_i \xi_i)$, where $\text{sign}(x)$ is the sign function. A perceptron can be used to classify inputs according to their respective labels (± 1 here). A statistical mechanics analysis revealed that the network can store up to a critical threshold of pattern density (or sample complexity) $\alpha \simeq 0.83$ [25], where $\alpha = \frac{M}{N}$ is the random-pattern (as inputs) density, and M is the number of random patterns. Instead of this classic random pattern storage setting, we consider learning task of random patterns with respective labels generated

by teacher networks (corresponding to different tasks). This is called the teacher-student setting [26, 27], where the student network learns to infer the teachers' rule embedded in the supplied data.

With increasing number of supplied learning examples, the size of the candidate-solution space of weights shrinks, and thus the generalization error on fresh data examples decreases. The statistical mechanics analysis also predicted that at $\alpha \simeq 1.245$, a first order phase transition to perfect generalization occurs [26, 27], which is the single-task learning. In our continual learning setting, we design two teacher networks with binary weights $\mathbf{W}^1 \in \{\pm 1\}^N$ and $\mathbf{W}^2 \in \{\pm 1\}^N$, respectively. Both teacher networks are ground truth for corresponding tasks. By definition, both teachers share an adjustable level of correlations in their weights, representing the similarity across tasks. In practice, their weights follow a joint distribution as

$$P(\mathbf{W}^1, \mathbf{W}^2) = \prod_{i=1}^N P_0(W_i^1, W_i^2) = \prod_{i=1}^N \left(\frac{1+r_0}{4} \delta(W_i^1 - W_i^2) + \frac{1-r_0}{4} \delta(W_i^1 + W_i^2) \right), \quad (1)$$

where $r_0 \in [-1, 1]$ denotes the task similarity. r_0 also denotes the overlap of the two teacher networks, since $r_0 = \frac{1}{N} \sum_{i=1}^N W_i^1 W_i^2$. The marginal joint probability $P_0(W_i^1, W_i^2)$ can be rewritten as $P_0(W_i^1, W_i^2) = p(W_i^1) p(W_i^2 | W_i^1)$, where $p(W_i^1) = \frac{1}{2} \delta(W_i^1 - 1) + \frac{1}{2} \delta(W_i^1 + 1)$, and $p(W_i^2 | W_i^1) = \frac{1+r_0}{2} \delta(W_i^1 - W_i^2) + \frac{1-r_0}{2} \delta(W_i^1 + W_i^2)$. To generate weights of the two teacher networks, we can first generate a set of random binary weights from the Rademacher distribution, and then flip the weight by a probability $\frac{1-r_0}{2}$. The random patterns for the two tasks are independently sampled from the Rademacher distribution as well, and then we have the training dataset $\{\mathbf{x}^{t,\mu}\}_{\mu=1}^{M_t}$, where the task index $t = 1, 2$. Given the sampled patterns, the teacher networks generate corresponding labels for each task, $\{y^{t,\mu}\}_{\mu=1}^{M_t}$. Hereafter, we use $\mathcal{D}_t = \{\mathbf{x}^{t,\mu}, y^{t,\mu}\}_{\mu=1}^{M_t}$, to denote the two datasets corresponding to the consecutive two tasks. The student network is another binary perceptron, whose goal is to learn the task rule provided by the teacher networks.

In the above setting, the student network shares the same structure (connection topology) with the two teacher networks, which implies that the student can not simultaneously learn both tasks perfectly, depending on the task similarity. However, this setting allows us to explore how the student adapts its weights to avoid catastrophic forgetting during learning of a new task, and how the network takes a trade-off between new and old knowledges in

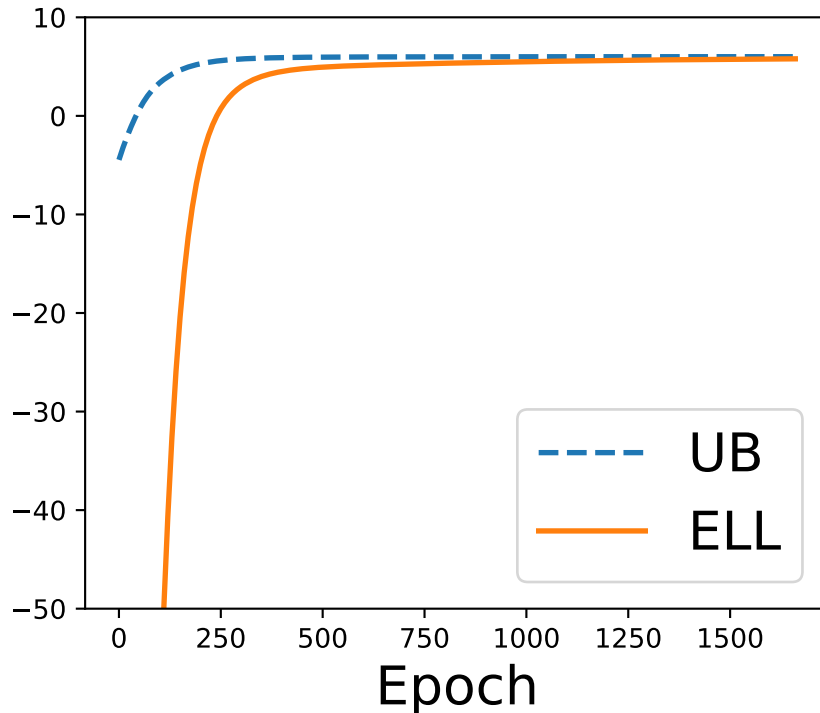


FIG. 1: Comparison between expected log-likelihood (ELL) and its upper bound (UB) in a simple network with 10 synapses and $M = 10$ examples to learn. In this case, ELL can be exactly computed by an exhaustive enumeration. For the numerical purpose, we use the surrogate $\Theta(x) = \lim_{\kappa \rightarrow \infty} \frac{e^{\kappa x}}{2 \cosh(\kappa x)}$. We take $\kappa = 10.0$. Equation (2) is used for ELL, while Eq. (3) is used for UB.

continual learning. Studying this simple system could also provide us insights about the continual learning in more complex applications, such as deep learning in real-world data.

B. Variational learning principle

Instead of training point weights, we consider learning the distribution of the weights in the sense that we train the student network to find an optimal distribution of weights [28]. Along this line, the variational method is an ideal framework for neural network learning [29, 30], since we can use simple trial distribution to approximate the original intractable weight distribution. The learning becomes then finding an optimal trial distribution parameterized by variational parameters [24].

In the first task, we introduce a variational distribution for synaptic weights, $q_{\theta}(\xi) = \prod_i \frac{e^{\beta \theta_i \xi_i}}{\cosh(\beta \theta_i)}$, where θ are variational parameters, and β is a hyperparameter. The optimal

distribution can be approximated by maximizing the expected log-likelihood

$$\boldsymbol{\theta}^* = \arg \max_{\boldsymbol{\theta}} \mathbb{E}_{q_{\boldsymbol{\theta}}} \ln P(\mathcal{D}_1 | \boldsymbol{\xi}). \quad (2)$$

Given an input \mathbf{x} , we choose the probability $P(\mathcal{D}_1 | \boldsymbol{\xi}) = P(y | \mathbf{x}, \boldsymbol{\xi})$ as $P(y | \mathbf{x}, \boldsymbol{\xi}) = \Theta\left(y \sum_{i=1}^N \xi_i x_i\right)$, where $\Theta(x)$ is the Heaviside function such that $\Theta(x) = 1$, if $x > 0$ and $\Theta(x) = 0$ otherwise. In practice, based on the Jensen's inequality, we actually update the variational parameters by maximizing the upper bound $\ln \mathbb{E}_{q_{\boldsymbol{\theta}}} P(\mathcal{D}_1 | \boldsymbol{\xi})$, which is less computationally challenging than the original one, and the optimization problem can then be formulated as

$$\begin{aligned} \boldsymbol{\theta}^* &= \arg \min_{\boldsymbol{\theta}} \{-\ln \mathbb{E}_{q_{\boldsymbol{\theta}}} P(\mathcal{D}_1 | \boldsymbol{\xi})\} \\ &= \arg \min_{\boldsymbol{\theta}} \left\{ -\ln \mathbb{E}_{q_{\boldsymbol{\theta}}} \prod_{\mu} \Theta\left(y^{\mu} \sum_{i=1}^N \xi_i x_i^{\mu}\right) \right\}. \end{aligned} \quad (3)$$

Maximizing the upper bound has been proved to be effective in unsupervised learning with many hidden neurons [30]. When the number of weights are about 10, the expected log-likelihood can be exactly computed, and we have checked that the bound could be tight (see Fig. 1). Based on the assumption of large N and the central limit theorem, Eq. (3) can be recast into the following form [29]

$$\boldsymbol{\theta}^* = \arg \min_{\boldsymbol{\theta}} \left\{ -\sum_{\mu} \ln H \left(-\frac{y^{\mu} \sum_i x_i^{\mu} \tanh \beta \theta_i}{\sqrt{\sum_i (1 - \tanh^2 \beta \theta_i)}} \right) \right\}, \quad (4)$$

where $H(x) = \int_x^{\infty} dz e^{-\frac{z^2}{2}} / \sqrt{2\pi} = \int_x^{\infty} \mathcal{D}z$, where $\mathcal{D}z$ denotes a standard Gaussian measure. Setting the loss function as $\mathcal{L} = -\sum_{\mu} \ln H \left(-\frac{y^{\mu} \sum_i x_i^{\mu} \tanh \beta \theta_i}{\sqrt{\sum_i (1 - \tanh^2 \beta \theta_i)}} \right)$, we can use the stochastic gradient descent (SGD)-based method to find a good trial distribution of weights, which may be a local or global minimum since the loss is a non-convex function. The gradients can be derived below,

$$\begin{aligned} \frac{\partial \mathcal{L}}{\partial \theta_j^t} &= \beta (\sigma_j^t)^2 \left(y \frac{x_j \sum_i (\sigma_i^t)^2 + \tanh(\beta \theta_j^t) \sum_i x_i \tanh(\beta \theta_i^t)}{(\sum_i (\sigma_i^t)^2)^{\frac{3}{2}}} \right. \\ &\quad \left. \times H' \left(-\frac{y \sum_i x_i \tanh(\beta \theta_i^t)}{\sqrt{\sum_i (1 - \tanh^2(\beta \theta_i^t))}} \right) \times H^{-1} \left(-\frac{y \sum_i x_i \tanh(\beta \theta_i^t)}{\sqrt{\sum_i (1 - \tanh^2(\beta \theta_i^t))}} \right) \right) \end{aligned} \quad (5)$$

where $\sigma_j^2 = 1 - \tanh^2(\beta\theta_j)$ captures the weight uncertainty, the data index μ is neglected, and t denotes the iterative time step. The synaptic plasticity is thus modulated by the weight uncertainty, which is biologically plausible [31] and bears the similarity with other heuristic strategies [8, 15]. Another salient feature is that, provided that the uncertainty of a weight is small, this weight can be less plastic because of encoding important information of previous tasks. In addition, the weight’s synaptic plasticity is also tuned by the total uncertainty of the network, $\sum_i(\sigma_i^t)^2$, which plays a role of global regularization.

During the second-task learning, the posterior distribution of weights becomes

$$P(\boldsymbol{\xi}|\mathcal{D}_1, \mathcal{D}_2) = \frac{P(\mathcal{D}_2|\boldsymbol{\xi}, \mathcal{D}_1)P(\boldsymbol{\xi}|\mathcal{D}_1)}{P(\mathcal{D}_2|\mathcal{D}_1)}. \quad (6)$$

We assume that when the student learns the second task, the knowledge from the first task becomes a prior constraining the subsequent learning, i.e., $P(\boldsymbol{\xi}|\mathcal{D}_1) \simeq q_{\boldsymbol{\theta}^1}(\boldsymbol{\xi})$, where $q_{\boldsymbol{\theta}^1}(\boldsymbol{\xi})$ is the variational distribution after learning the first task. We model the posterior of weights during learning of the second task as $q_{\boldsymbol{\theta}^2}(\boldsymbol{\xi}) = \prod_i \frac{e^{\beta\theta_i^2\xi_i}}{\cosh(\beta\theta_i^2)}$. Optimal variational parameters can be obtained by minimizing the Kullback-Leibler (KL) divergence between variational distribution and posterior distribution [30],

$$\begin{aligned} \boldsymbol{\theta}^{2*} &= \arg \min_{\boldsymbol{\theta}^2} \mathbb{E}_{q_{\boldsymbol{\theta}^2}} \ln \frac{q_{\boldsymbol{\theta}^2}(\boldsymbol{\xi})}{P(\boldsymbol{\xi}|\mathcal{D}_1, \mathcal{D}_2)} \\ &= \arg \min_{\boldsymbol{\theta}^2} \mathbb{E}_{q_{\boldsymbol{\theta}^2}} \ln \frac{q_{\boldsymbol{\theta}^2}(\boldsymbol{\xi})}{q_{\boldsymbol{\theta}^1}(\boldsymbol{\xi})} - \mathbb{E}_{q_{\boldsymbol{\theta}^2}} \ln P(\mathcal{D}_2|\boldsymbol{\xi}) \\ &\simeq \arg \min_{\boldsymbol{\theta}^2} \text{KL}\left(q_{\boldsymbol{\theta}^2}(\boldsymbol{\xi})||q_{\boldsymbol{\theta}^1}(\boldsymbol{\xi})\right) - \ln \mathbb{E}_{q_{\boldsymbol{\theta}^2}} P(\mathcal{D}_2|\boldsymbol{\xi}), \end{aligned} \quad (7)$$

where we discard $P(\mathcal{D}_2|\mathcal{D}_1)$ because this term does not depend on the model parameters, and we use $P(\mathcal{D}_2|\boldsymbol{\xi}, \mathcal{D}_1) = P(\mathcal{D}_2|\boldsymbol{\xi})$, and we also approximate the objective function \mathcal{L} by minimizing the lower bound of the KL divergence (in other words, we train the network to make the bound as tight as possible). We remark here that one can also minimize the KL divergence between a trial probability $q_{\boldsymbol{\theta}}$ and the posterior $P(\boldsymbol{\xi}|\mathcal{D}_1)$ for the first-task learning [see Eq. (2)], which would require a prior probability of $\boldsymbol{\xi}$. Even if we set this prior to a uniform one, the system exhibits a similar learning behavior but the learning becomes harder as more data samples are required for reaching the same low generalization error with the learning using Eq. (2). Therefore, we use Eq. (2) as our first-task learning framework.

The first term in Eq. (7) is a regularized term that makes the network to maintain the learned information of the first task. The second term is the expected log-likelihood term that leads the network to explain new data. The SGD-based method can then be applied to obtain the optimal solution (local or global minimum). The gradient can be computed as,

$$\begin{aligned} \frac{\partial \mathcal{L}}{\partial \theta_j^{2,t}} &= \beta(\sigma_j^{2,t})^2 \left(\beta(\theta_j^{2,t} - \theta_j^1) + y \frac{x_j \sum_i (\sigma_i^{2,t})^2 + \tanh(\beta\theta_j^{2,t}) \sum_i x_i \tanh(\beta\theta_i^{2,t})}{(\sum_i (\sigma_i^{2,t})^2)^{\frac{3}{2}}} \right. \\ &\quad \left. \times H' \left(-\frac{y \sum_i x_i \tanh(\beta\theta_i^{2,t})}{\sqrt{\sum_i (1 - \tanh^2(\beta\theta_i^{2,t}))}} \right) \times H^{-1} \left(-\frac{y \sum_i x_i \tanh(\beta\theta_i^{2,t})}{\sqrt{\sum_i (1 - \tanh^2(\beta\theta_i^{2,t}))}} \right) \right), \end{aligned} \quad (8)$$

where \mathcal{L} is the objective function to minimize in Eq. (7), and the data index is neglected and must refer to the task 2, and the gradient is still modulated by the weight uncertainty. Compared to the gradient of the first-task learning, the additional term comes from the KL divergence term. This term encourages the network to remember the first-task information. Therefore, this synaptic plasticity rule expresses the competition between old and new tasks (the second term). This trade-off allows the network to maintain the old knowledge but still adapt to the new task, thereby avoiding catastrophic forgetting to some extent.

We first show the simulation performance of our toy variational continual learning setting. In Fig. 2 (a), with increasing amount of provided examples, the single-task learning performance improves. In Fig. 2 (b), when the task transition occurs, the test error of the first task increases, yet finally achieving a stable value across training. The test error of the second task decreases, but can not achieve the error level that can be reached when the task is trained in isolation [Fig. 2(c)]. This is because the network does not forget the distinct characteristics of the first task completely, due to the regularization term. The lower test error would be achieved given more training examples for the second task. Figure 2 (d) illustrates the effect of the KL term, where we plot the overlap between the student inference and the common part of both teachers. Without the KL term, the overlap falls more sharply and then increases more rapidly, while the presence of the KL term makes the overlap change relatively slowly. This suggests that, the KL term makes the network tend to protect the first task from a fast forgetting (see the poor performance of the traditional SGD in continual learning in Fig. 2(b,c)]. The lower overlap (but still closer to one) allows more flexibility to balance the continual learning.

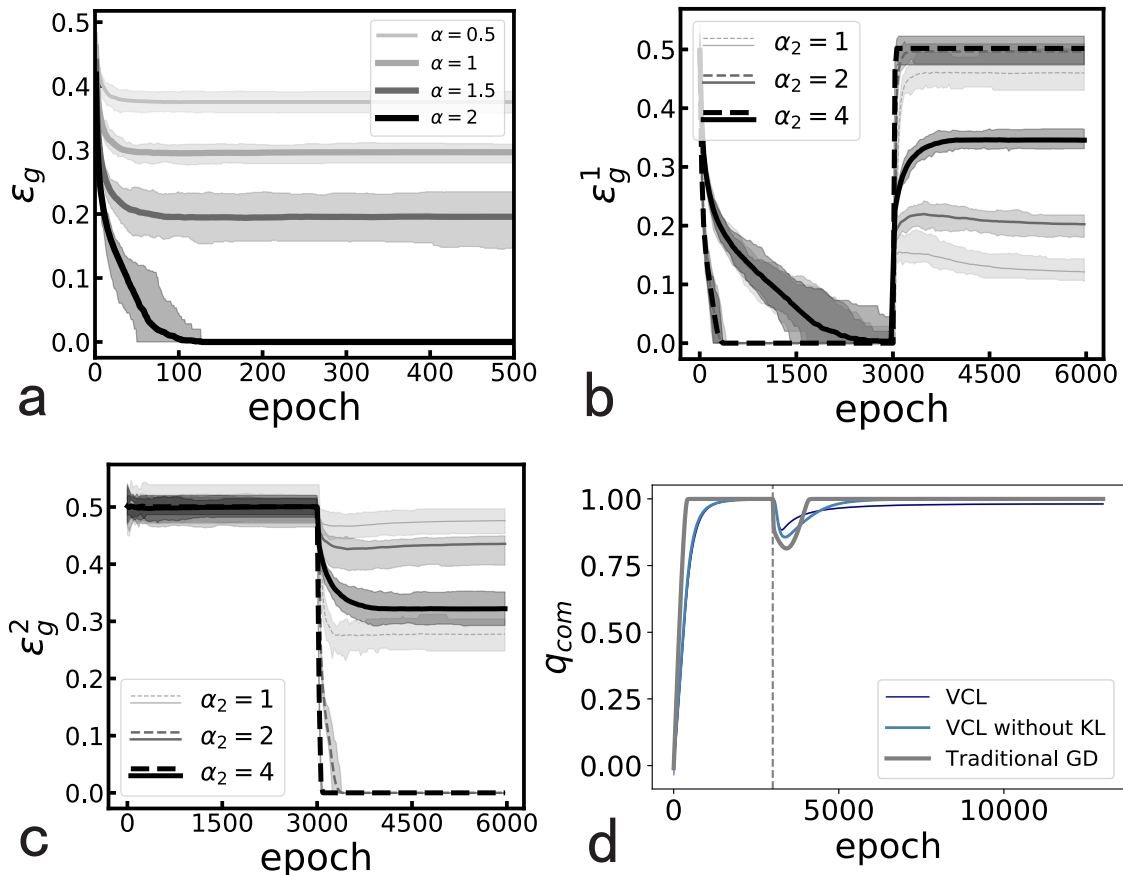


FIG. 2: Learning performance of the toy model. (a) Test error of the first task with different α . (b) Test error of the first task. (c) Test error of the second task. In (b,c), the task transition occurs at the 3000-th epoch, and $r_0 = 0$. $\alpha_1 = 2$, but α_2 varies. Results are averaged over 20 trials. (d) The overlap q_{com} between the student weights and the common part of both teachers (task similarity). $q_{\text{com}} = \frac{1}{N_{\text{com}}} \sum_i \hat{m}_i \hat{W}_i$, where \hat{m}_i denotes the student's magnetization of the i -th synaptic weight and we choose i such that $W_i^1 = W_i^2 (= \hat{W}_i)$. N_{com} denotes the total number of common weights in both teachers. In simulations, $r_0 = 0.5$, $\alpha_1 = 3$ and $\alpha_2 = 4$. For the traditional (full batch) GD algorithm, the optimization for two tasks is in the magnetization space (see Eq. (10) for the first task, and the second task has a similar form), and no KL divergence terms are used. The other two algorithms are implemented in the field (θ) space. The task switch (the dashed line) occurs at the 3000-th epoch. The network size $N = 1000$. For (a,b,c), SGD is applied. For (d), the full batch GD is used. The performance of the traditional SGD (dashed lines) is also shown in (b,c) for comparison.

We next derive the mean-field theory to evaluate analytically the continual learning performance.

C. Mean-field theory: Franz-Parisi Potential

Mean-field theory is a powerful tool for analyzing complex systems in statistical physics. In the previous section, we describe the variational method in training the binary perceptron to realize continual learning. In this section, we derive mean-field theory to analyze the variational continual learning. Instead of the local fields θ^1 and θ^2 (useful for practical training due to their unbounded values), we parameterize the variational distribution with weight-magnetization $m_{1,i} = \tanh \beta\theta_i^1$ and $m_{2,i} = \tanh \beta\theta_i^2$, for the sake of analytical studies. The variational distributions are specified respectively by

$$\begin{aligned} Q_{m_1}(\boldsymbol{\xi}) &= \prod_{i=1}^N \frac{1 + \xi_i m_{1,i}}{2}, \\ Q_{m_2}(\boldsymbol{\xi}) &= \prod_{i=1}^N \frac{1 + \xi_i m_{2,i}}{2}, \end{aligned} \tag{9}$$

where $m_{1,i}, m_{2,i} \in [-1, 1]$ are the magnetization of the i^{th} synaptic weight in the first and second task learning respectively. We perform the statistical mechanics analysis on the two-task learning, with the goal of extracting the role of model parameters (e.g., sample complexity, task similarity and so on) in the continual learning.

1. The first-task analysis

To perform the mean field theory analysis of the first-task learning, we define the loss function in the variational method as the Hamiltonian,

$$\mathcal{L}_1(\mathbf{m}) = - \sum_{\mu=1}^{M_1} \ln H \left(- \frac{y^\mu \sum_i m_i x_i^{1,\mu}}{\sqrt{\sum_i (1 - m_i^2)}} \right), \tag{10}$$

where $y^\mu = \text{sign}(\sum_i W_i^1 x_i^{1,\mu})$ is the label generated by the teacher network. The Boltzmann distribution reads

$$P(\mathbf{m}) = \frac{1}{Z} e^{-\beta \mathcal{L}_1(\mathbf{m})}, \tag{11}$$

where β is an inverse temperature, $Z = \int_{\Omega} \prod_i dm_i e^{-\beta \mathcal{L}_1(\mathbf{m})}$ is the partition function and the integral domain $\Omega = [-1, 1]^N$. To obtain the equilibrium properties, we should first compute

the disorder-averaged free energy (or the log-partition-function), which can be achieved by using the replica trick. The replica trick proceeds as $\langle \ln Z \rangle = \lim_{n \rightarrow 0} \frac{\ln \langle Z^n \rangle}{n}$, where $\langle \cdot \rangle$ denotes the average over the quenched disorder. Then, we have

$$\langle Z^n \rangle = \int_{\Omega^n} \prod_{a=1}^n \prod_{i=1}^N dm_i^a \left\langle \prod_{a=1}^n \prod_{\mu=1}^{M_1} H^\beta \left(-\frac{\text{sign}(\sum_i W_i^1 x_i^{1,\mu}) \sum_i m_i^a x_i^{1,\mu}}{\sqrt{\sum_i 1 - (m_i^a)^2}} \right) \right\rangle. \quad (12)$$

Under the replica symmetric (RS) Ansatz (detailed in the appendix C), the free energy density at a given data density $\alpha = \frac{M}{N}$ is given by

$$-\beta f_{\text{RS}} = \lim_{n \rightarrow 0, N \rightarrow \infty} \frac{\ln \langle Z^n \rangle}{nN} = \lim_{n \rightarrow 0} -\frac{1}{2} (\hat{q}_d q_d + (n-1) \hat{q}_0 q_0) - \hat{r}_1 r_1 + \frac{\ln G_{\text{S}}}{n} + \alpha_1 \frac{\ln G_{\text{E}}}{n}, \quad (13)$$

where

$$\begin{aligned} G_{\text{E}} &= \int \mathcal{D}z \, 2H \left(-\frac{r_1}{\sqrt{q_0 - r_1^2}} z \right) \left(\int \mathcal{D}\sigma \, H^\beta \left(-\frac{\sqrt{q_d - q_0} \sigma + \sqrt{q_0} z}{\sqrt{1 - q_d}} \right) \right)^n, \\ G_{\text{S}} &= \int \mathcal{D}z \left(\int_{-1}^{+1} dm \, e^{\frac{1}{2} \hat{q}_d m^2 - \frac{1}{2} \hat{q}_0 m^2 + \sqrt{\hat{q}_0} m z + \hat{r}_1 m} \right)^n. \end{aligned} \quad (14)$$

Order parameters are introduced as $q_0 = \frac{1}{N} \sum_i m_i^a m_i^b$ for $a \neq b$ indicating the overlap of different equilibrium states, $q_d = \frac{1}{N} \sum_i m_i^a m_i^a$ indicating the self-overlap of states (the self-overlap relates to the size of valid weight space $\hat{\sigma} = 1 - q_d$), and finally $r_1 = \frac{1}{N} \sum_i m_i W_i^1$ indicating the overlap between the student's inference and the teacher's ground truth. In practice, q_d can be also estimated from the gradient descent dynamics during training, and we use q_* to denote this measure, i.e., $q_*(t) = \frac{1}{N} \sum_i (m_i(t))^2$, and $\Delta m_i(t) \propto \partial_{m_i} \mathcal{L}_1(\mathbf{m})$. $\{\hat{q}_0, \hat{q}_d, \hat{r}_1\}$ are the conjugated order parameters introduced by the Fourier transform. These order parameters can be obtained by solving saddle point equations (detailed in appendix C). To evaluate the learning performance, we define the generalization error $\epsilon_g^1 = \langle \mathbb{E}_{\mathbf{x}^*} \Theta(-y^* \hat{y}^*) \rangle$, where (\mathbf{x}^*, y^*) is the fresh data sample, and \hat{y}^* is the student's prediction, and $\langle \cdot \rangle$ denotes the disorder average. The test error can be calculated as (see details in appendix C)

$$\epsilon_g^1 = \int \mathcal{D}z \, 2H \left(-\frac{p_1}{\sqrt{1 - p_1^2}} z \right) \Theta(-z) = \frac{1}{\pi} \arccos(p_1), \quad (15)$$

where $p_1 = \frac{1}{N} \sum_i \text{sign}(m_i) W_i^1$ denotes the overlap between the decoded weights and the

teacher’s weights, and can be obtained by solving the saddle point equations as well.

We first show how order parameters change with respect to the data density α . As defined, q_d signals the size of the valid weight space. As the sample complexity increases, the weight space shrinks down to a single point representing the ground truth [Fig. 3 (a)]. As shown in Fig. 3 (b), the stochastic gradient descent dynamics results are approximately consistent with the theoretical predictions (at least qualitatively). The deviations may be caused by the fact that the SGD could be trapped by local minima (suboptimal solutions) of the variational energy landscape. But for a fixed α , we can dynamically rescaled the norm of \mathbf{m} after every update (slow type SGD [29]), and compare the dynamical ϵ_g^1 with its equilibrium counterpart (with the same value of q_*). We find that the SGD results are comparable with the equilibrium predictions, at least qualitatively [Fig. 3 (d)]. The deviation may be caused by the finite size effects (see also the previous work [29]).

In particular, Fig. 3 (b) reveals a continuous phase transition (from poor to perfect generalization) in the variational parameter space (despite a binary perceptron learning considered in our setting). Due to the numerical accuracy of the replica results at a large α , we find that after $\alpha = 1.7$, a power law scaling of the generalization error with a large exponent [~ 13.1 , see the inset of Fig. 3 (b)] is observed. We remark that the SGD could reach zero error (perfect generalization) after $\alpha_c \simeq 1.7$, while the replica result obtained at a large $\beta = 20$ has a fast decay (lower than 10^{-2}) after α_c [see the inset of Fig. 3 (b)]. It is expected that the replica prediction of the generalization error will reach lower values with increasing β , which requires a huge number of Monte-Carlo samples to get an accurate estimate of the integral in Eq. (15) and also in solving the saddle-point equations (see details in appendix C). The power-law fitting for the error below 10^{-3} may thus be unreliable. We conclude that in the zero temperature limit, the perfect generalization is conjectured to be achievable, although a high β may lead to replica symmetry breaking [29]. We could alternatively estimate the transition threshold by analyzing the convergence time of the learning algorithm [Fig. 3 (c)]. The convergence time is peaked at $\alpha_c \simeq 1.7$, which is in stark contrast to the case of training in the direct binary-weight space [26, 27], which leads to a discontinuous transition at $\alpha_c = 1.245$ (a spinodal point locates at $\alpha_{sp} = 1.492$). This suggests that the variational learning erases the metastable regime where the poor generalization persists until the spinodal point. Thus the variational framework bears optimization benefits for learning in neural networks with discrete weights.

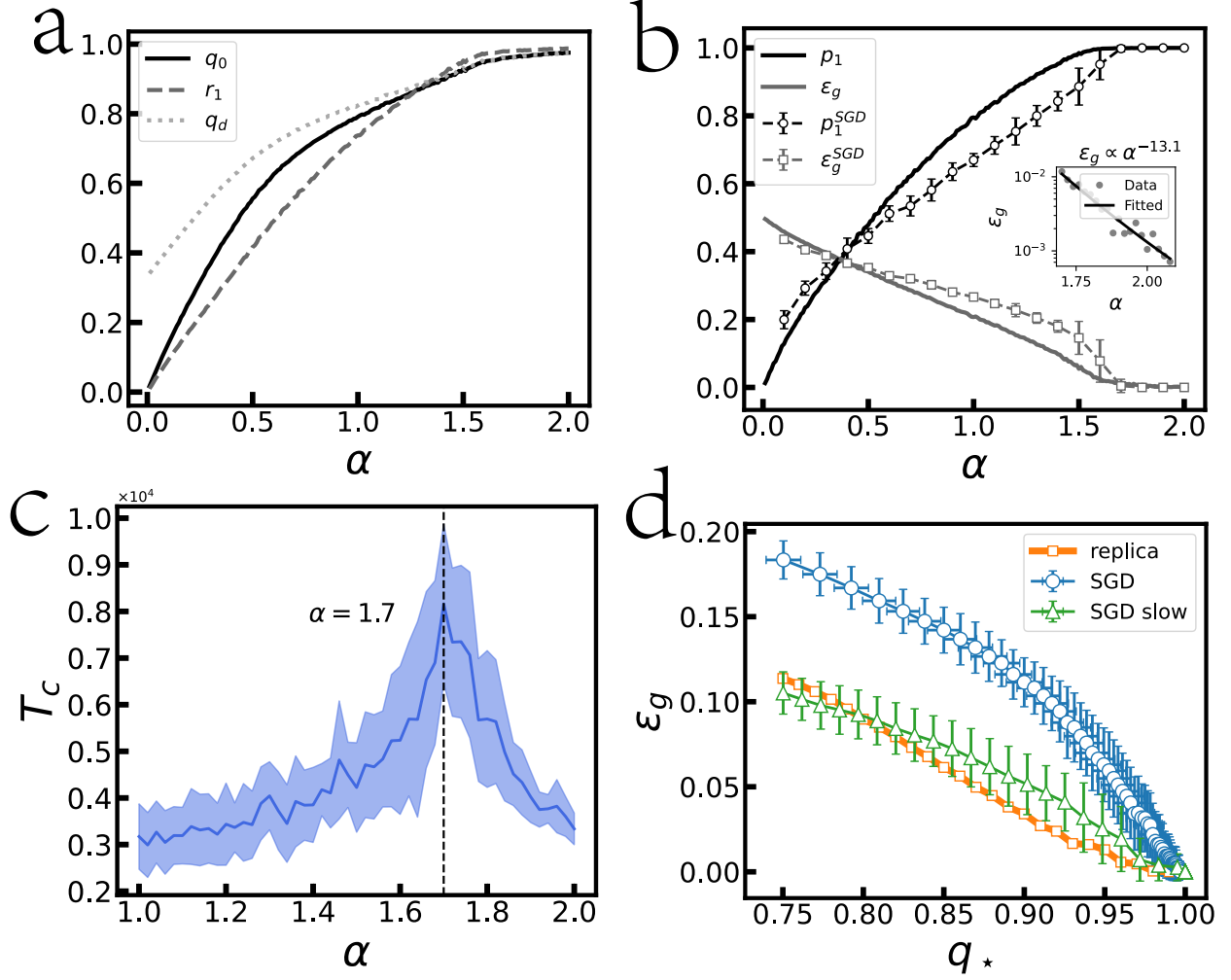


FIG. 3: Mean-field results of the first-task learning compared with SGD simulations. (a) The order parameters versus data density α ($\beta = 20$). (b) Generalization error versus data density ($\beta = 20$). The connected symbols represent the result of SGD. The inset shows a power-law scaling for replica results when $\alpha \geq 1.7$. The symbol (Data) in the inset is the replica theory. (c) Convergence time step T_c of the full batch gradient descent simulation. T_c is recorded when the drop of ϵ_g during $[T_c, T_c + 1000]$ starts to be less than 0.0005. The convergence time peaks at $\alpha = 1.7$. The results are averaged over 20 trials (network size $N = 3\,000$). (d) Generalization error versus quenched q_* ($\alpha = 2$). The slow SGD means a rescale of the norm of m to q_* after each update. The results of SGD are averaged over 20 trials (network size $N = 1\,000$).

2. The second-task analysis

Similarly, we specify the second-task Hamiltonian as follows,

$$\mathcal{L}_2(\mathbf{m}) = - \sum_{\mu=1}^{M_2} \ln H \left(- \frac{\text{sign}(\sum_i W_i^2 x_i^{2,\mu}) \sum_i m_i x_i^{2,\mu}}{\sqrt{\sum_i (1 - m_i^2)}} \right) + \sum_{i=1}^N \text{KL}(Q_{m_i} \| Q_{m_{1,i}}). \quad (16)$$

As explained before, the first term is a reconstruction term that maximizes the log-likelihood of the second-task data, and the second term prevents the network from forgetting the previously acquired knowledge. Due to the regularization term, we have to treat the equilibrium analysis differently from the single task learning. It is natural to put the analysis within the Franz-Parisi potential framework [22, 23]. More precisely, we define the potential for the second-task learning as

$$\Phi = \frac{1}{\bar{Z}} \int_{\tilde{\Omega}} \prod_{i=1}^N d\tilde{m}_i e^{-\tilde{\beta}\mathcal{L}_1(\tilde{\mathbf{m}})} \ln \int_{\Omega} \prod_{i=1}^N dm_i e^{-\beta\mathcal{L}_2(\mathbf{m}, \tilde{\mathbf{m}})}. \quad (17)$$

Taking the replica symmetric (RS) Ansatz, the disorder averaged potential is related to the following action \mathcal{S} (see details in appendix C),

$$\begin{aligned} \mathcal{S} = \lim_{n \rightarrow 0} \lim_{s \rightarrow 0} & -\frac{1}{2} \left(n\hat{q}_d\tilde{q}_d + s(s-1)\hat{q}_0q_0 \right) - \frac{1}{2} (s\hat{q}_dq_d + n(n-1)\hat{q}_0q_0) - n\hat{r}_1\tilde{r}_1 - s\hat{r}_2r_2 \\ & + \ln \mathcal{G}_S + \alpha_1 \ln \mathcal{G}_E^1 + \alpha_2 \ln \mathcal{G}_E^2, \end{aligned} \quad (18)$$

where

$$\begin{aligned} \mathcal{G}_E^1 &= \left\langle \prod_{a=1}^n H^{\tilde{\beta}} \left(-\frac{\text{sign}(\tilde{v}_1)\tilde{u}^a}{\sqrt{1-\tilde{q}_{aa}}} \right) \right\rangle \\ &= \int \mathcal{D}z \, 2H \left(-\frac{\tilde{r}_1}{\sqrt{\tilde{q}_0 - \tilde{r}_1^2}} z \right) \left(\int \mathcal{D}\sigma \, H^{\tilde{\beta}} \left(-\frac{\sqrt{\tilde{q}_d - \tilde{q}_0}\sigma + \sqrt{\tilde{q}_0}z}{\sqrt{1-\tilde{q}_d}} \right) \right)^n, \end{aligned} \quad (19)$$

and

$$\begin{aligned} \mathcal{G}_E^2 &= \left\langle \prod_{c=1}^s H^{\beta} \left(-\frac{\text{sign}(v_2)u^c}{\sqrt{1-q_{cc}}} \right) \right\rangle \\ &= \int \mathcal{D}z \, 2H \left(-\frac{r_2}{\sqrt{q_0 - r_2^2}} z \right) \left(\int \mathcal{D}\sigma \, H^{\beta} \left(-\frac{\sqrt{q_d - q_0}\sigma + \sqrt{q_0}z}{\sqrt{1-q_d}} \right) \right)^s, \end{aligned} \quad (20)$$

and

$$\begin{aligned} \mathcal{G}_S &= \frac{1+r_0}{2} \int \mathcal{D}z_1 \left(\int_{-1}^{+1} d\tilde{m} e^{\tilde{\mathcal{I}}(\tilde{m}, z_1)} \right)^{n-1} \int_{-1}^{+1} d\tilde{m} e^{\tilde{\mathcal{I}}(\tilde{m}, z_1)} \int \mathcal{D}z_2 \left(\int_{-1}^{+1} dm e^{\mathcal{J}^+(m, \tilde{m}, z_2)} \right)^s \\ &+ \frac{1-r_0}{2} \int \mathcal{D}z_1 \left(\int_{-1}^{+1} d\tilde{m} e^{\tilde{\mathcal{I}}(\tilde{m}, z_1)} \right)^{n-1} \int_{-1}^{+1} d\tilde{m} e^{\tilde{\mathcal{I}}(\tilde{m}, z_1)} \int \mathcal{D}z_2 \left(\int_{-1}^{+1} dm e^{\mathcal{J}^-(m, \tilde{m}, z_2)} \right)^s. \end{aligned} \quad (21)$$

Note that, \tilde{v}_1 and v_2 are related to quenched disorder (see appendix C), $\{q_0, r_2, q_d\}$ are order parameters in parallel to the first-task learning, while $\{\tilde{q}_0, \tilde{r}_1, \tilde{q}_d\}$ can be obtained by solving the single-task saddle point equations (inherited from the first-task analysis). The functions $\tilde{\mathcal{I}}$ and \mathcal{J}^\pm are defined in appendix C. The test error of the second task can be derived in the form,

$$\epsilon_g^2 = \int \mathcal{D}z \, 2H\left(-\frac{p_2}{\sqrt{1-p_2^2}}z\right) \Theta(-z) = \frac{1}{\pi} \arccos(p_2), \quad (22)$$

where $p_2 = \frac{1}{N} \sum_i \text{sign}(m) W_i^2$ denote the overlap between the decoded weights and the second-teacher weights. Similarly, the test error of the first-task after learning both tasks is given by

$$\epsilon_g^1 = \int \mathcal{D}z \, 2H\left(-\frac{p_1}{\sqrt{1-p_1^2}}z\right) \Theta(-z) = \frac{1}{\pi} \arccos(p_1), \quad (23)$$

where $p_1 = \frac{1}{N} \sum_i \text{sign}(m_i) W_i^1$.

We finally study the theoretically predicted performances compared with numerical simulations. In Fig. 4 (a), we find that the task similarity strongly impacts the learning performance of the second task. When r_0 takes a negative value, the learning becomes much harder, as more data examples are required to decrease the generalization error, while a positive task similarity makes the learning of the second task easier. The SGD results match well with the theoretical prediction, except for the region around the transition, which may call for longer simulation time in searching for good solutions. As expected, the generalization of the first task will increase during learning the second task [Fig. 4 (b)], which is due to the fact that both tasks share a partial similarity (i.e., not completely the same). We also multiply the KL term by a factor γ , and study the effect of this term by tuning down this factor [e.g., $\gamma = 0.1$ in Fig. 4 (c,d)]. We find that the learning of the second task becomes fast as less data examples are required, and the critical value of α is also impacted. Furthermore, the memorization of the first task is strongly degraded. This result is consisted with that found in Fig. 2 (d).

For a numerical verification of the mean-field replica theory, we train a perceptron with the number of synapses $N = 5000$. The learning rate equals to 0.001 for the whole training process. If we use SGD, the size of a mini-batch is set to 32. In the replica analysis, the hyperparameter $\beta_1 = \beta_2 = 20$ for the first and second tasks. Once the algorithm for the present task converges (e.g., the accuracy is stable), we shift the learning to a new task.

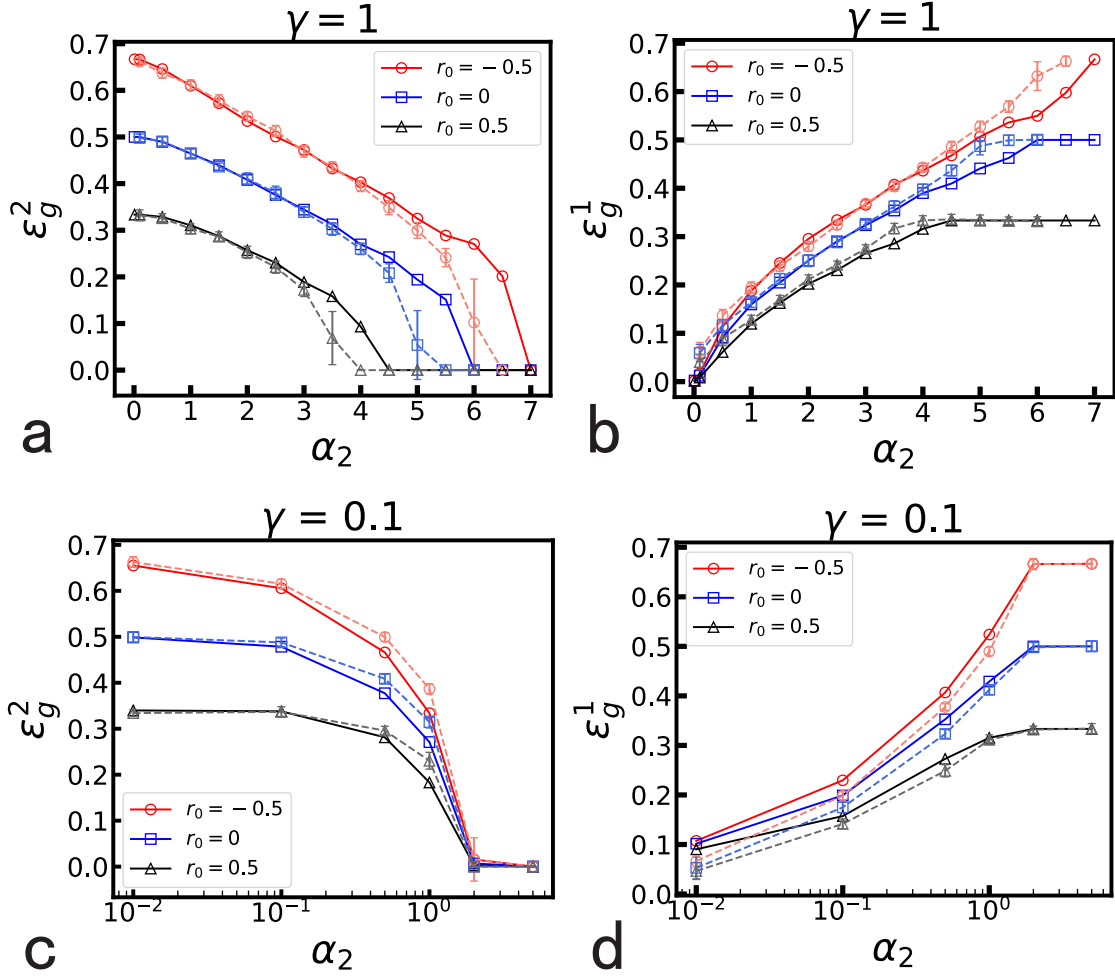


FIG. 4: Generalization versus α for the variational continual learning. The symbols connected by dashed lines are simulation results of GD (twenty trials are averaged), while those connected by full lines are replica predictions. $\alpha_1 = 2$, $N = 1000$, and different learning rates are used for different values of α_2 . Different task similarities are considered. The KL term is multiplied by a tuning factor γ . (a,b) $\gamma = 1.0$. (c,d) $\gamma = 0.1$.

Figure 5 shows an excellent agreement between equilibrium predictions obtained by replica analysis and real training of perceptrons.

III. CONTINUAL LEARNING IN DEEP NEURAL NETWORKS

Catastrophic forgetting is an unfavored property for deep neural networks applied to continual learning or multi-task learning. In this section, we extend the variational methods for the toy binary perceptron to deep neural networks in classifying structured dataset.

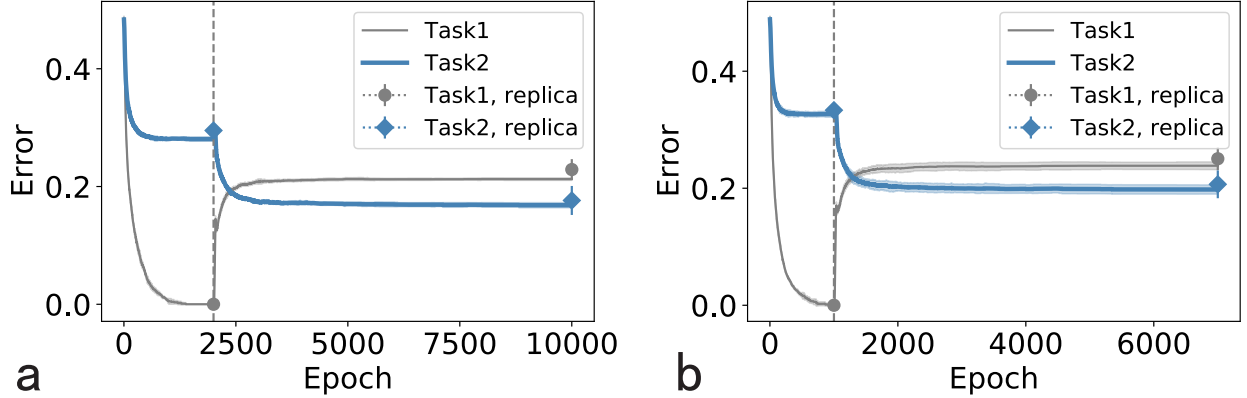


FIG. 5: The comparison between replica results and simulation in perceptron. The simulation results are averaged over five independent trials. The solid line shows the accuracy obtained from training the perceptron, while the symbols indicate the replica results. The dashed line indicates the task switch. (a) $r_0 = 0.6$, and $\alpha_1 = \alpha_2 = 3.0$. (b) $r_0 = 0.5$, $\alpha_1 = 4.0$, and $\alpha_2 = 3.0$.

A. Variational learning principle

Variational learning principle is a popular variational Bayesian framework applied in a wide range of scenarios [12–15], which focus mainly on deep networks with real-valued weights. To learn a computationally efficient (binary weights) deep network, we adapt the variational principle to the continual learning, in theory and practical training, comparing the performance with that of the heuristic metaplasticity algorithm [8], a unique available method for comparison in our current context. Within this framework, the posterior of parameters \mathbf{w} is learned from T continually presented datasets $\{\mathbf{x}_t^{(n)}, \mathbf{y}_t^{(n)}\}_{n=1}^{N_t}$, where t denotes the task index ranging from 1 to T , and N_t denotes the size of dataset t . When the multi-task data examples are sequentially shown to the machine, the posterior distribution of \mathbf{w} is denoted as $p(\mathbf{w}|\mathcal{D}^k)$, after k -th training steps based on the dataset \mathcal{D}^k (minibatch at the k -th step), can be calculated using the Bayes' rule as $p(\mathbf{w}|\mathcal{D}^k) = \frac{p(\mathcal{D}^k|\mathbf{w})p(\mathbf{w})}{p(\mathcal{D}^k)}$. The prior $p(\mathbf{w})$ depends on the $(k-1)$ -th step, which can be taken to be the posterior in the previous training step $p(\mathbf{w}(k-1)|\mathcal{D}^{k-1})$. Taken together, the posterior $p(\mathbf{w} | \mathcal{D})$ can be written as

$$p(\mathbf{w}|\mathcal{D}^k) = \frac{p(\mathcal{D}^k|\mathbf{w})p(\mathbf{w}(k-1)|\mathcal{D}^{k-1})}{p(\mathcal{D}^k)}. \quad (24)$$

Unfortunately, the difficulty here is that the posterior is typically intractable for most of probabilistic models, which thereby requires an application of the variational method. We approximate the true posterior with a tractable distribution parameterized by the variational

parameter θ . By updating θ , we approach the target distribution as close as possible.

Given a simple trial probability distribution over the latent variable \mathbf{w} parameterized by θ , i.e., $q_\theta(\mathbf{w})$, the minimization of the KL divergence between $q_\theta(\mathbf{w})$ and $p(\mathbf{w}|\mathcal{D})$ results in the following solution

$$\theta^* = \arg \min_{\theta} \text{KL} [q_\theta(\mathbf{w}) \| p(\mathbf{w}|\mathcal{D})]. \quad (25)$$

Therefore, we can define the loss function \mathcal{L} as

$$\mathcal{L} = \text{KL} [q_\theta(\mathbf{w}) \| p(\mathbf{w}|\mathcal{D})] = \mathcal{L}_{reg} + \mathcal{L}_{rec}, \quad (26)$$

where we replace the prior $p(\mathbf{w})$ with the variational posterior in the previous time step $q_{\theta^{k-1}}(\mathbf{w})$, and we define the regularization term $\mathcal{L}_{reg} = \text{KL} [q_{\theta^k}(\mathbf{w}) \| q_{\theta^{k-1}}(\mathbf{w})]$, and the reconstruction term $\mathcal{L}_{rec} = -\mathbb{E}_{q_{\theta^k}(\mathbf{w})} [\ln p(\mathcal{D}|\mathbf{w})]$. The term \mathcal{L}_{rec} computes the averaged log-likelihood of the network output, which can be crudely approximated by considering a single sample \mathbf{w}_s of $q_{\theta^k}(\mathbf{w})$ from a rough Monte-Carlo sampling estimation. By computing gradients of θ on this loss function \mathcal{L} , we arrive at

$$\begin{aligned} \frac{\partial \mathcal{L}}{\partial \theta_i^k} &= \sum_{w_i} \frac{\partial q_{\theta_i^k}(w_i)}{\partial \theta_i^k} \left(1 - \ln q_{\theta_i^k}(w_i) - \ln q_{\theta_i^{k-1}}(w_i) \right) \\ &\quad - \frac{\partial \ln p(\mathcal{D} | \mathbf{w}_s)}{\partial \theta_i^k}. \end{aligned} \quad (27)$$

Learning of the variational parameter θ_i can be achieved by a gradient descent of the objective function, i.e.,

$$\theta_i^{k+1} = \theta_i^k - \eta \frac{\partial \mathcal{L}}{\partial \theta_i^k}, \quad (28)$$

where η denotes the learning rate, and θ_i^k refers to the i -th connection in one layer a deep network (e.g., $\theta_{ij}^{l,k}$ for the connection (ij) at layer l below).

We consider a deep neural network with L layers, and N_l denotes the width of l th layer. w_{ij}^l indicates the weight connecting neuron i at the upstream layer l to neuron j at the downstream layer $l + 1$. The state of neuron j at the $l + 1$ th layer h_j^{l+1} is a non-linear transformation of the preactivation $z_j^{l+1} = \frac{1}{\sqrt{N_l}} \sum_i w_{ij}^l h_i^l$. The transfer function $f(\cdot)$ for layers $l = 1, 2, \dots, L - 1$ is chosen to be the rectified linear unit (ReLU), which is defined as $f(z) = \max(0, z)$. For the output layer, the softmax function $h_k = e^{z_k} / \sum_i e^{z_i}$ is used, specifying

the probability over all classes of the input images, where z_i is the preactivation of neuron i at the output layer. The supervised learning is considered, where \hat{h}_k indicates the target of h_k^l , and the cross entropy $\mathcal{L}_{ce} = -\sum_i \hat{h}_i \ln h_i$ is used as a cost function corresponding to \mathcal{L}_{rec} . In our setting, a double-peak distribution is applied to model the binary weight as $q_{\theta_{ij}^l}(w_{ij}^l) = \frac{e^{\beta w_{ij}^l \theta_{ij}^l}}{e^{\beta \theta_{ij}^l} + e^{-\beta \theta_{ij}^l}}$, where β is a hyperparameter, and the field-like parameter θ_{ij} controls the probability distribution of w_{ij} as $q_{\theta_{ij}^l}(+1) = \frac{e^{\beta \theta_{ij}^l}}{e^{\beta \theta_{ij}^l} + e^{-\beta \theta_{ij}^l}}$ and $q_{\theta_{ij}^l}(-1) = \frac{e^{-\beta \theta_{ij}^l}}{e^{\beta \theta_{ij}^l} + e^{-\beta \theta_{ij}^l}}$. Therefore, the gradients of θ on \mathcal{L}_{reg} can be computed as

$$\begin{aligned} & \frac{\partial \text{KL} \left[q_{\theta_{ij}^{l,k}}(w_{ij}^{l,k}) \| q_{\theta_{ij}^{l,k-1}}(w_{ij}^{l,k-1}) \right]}{\partial \theta_{ij}^{l,k}} \\ &= \beta^2 \left(\theta_{ij}^{l,k} - \theta_{ij}^{l,k-1} \right) \left(\sigma_{ij}^{l,k} \right)^2 = \beta^2 \left(\sigma_{ij}^{l,k} \right)^2 \Delta_{ij}^{l,k}, \end{aligned} \quad (29)$$

where the superscript l and k denote the layer index and iteration step respectively, and we define $\Delta_{ij}^{l,k}$ as the increments of the variational parameter $\Delta_{ij}^{l,k} = \theta_{ij}^{l,k} - \theta_{ij}^{l,k-1}$ between two successive steps. $\left(\sigma_{ij}^{l,k} \right)^2$ indicates the variance of w_{ij}^l as $\left(\sigma_{ij}^{l,k} \right)^2 = 1 - \tanh^2 \left(\beta \theta_{ij}^{l,k} \right)$, and thus captures the synaptic uncertainty.

To derive the gradients of \mathcal{L}_{rec} , we apply the mean-field method [28]. The first and second moments of w_{ij}^l are given by $\mu_{ij}^l = \langle w_{ij}^l \rangle = \tanh \left(\beta \theta_{ij}^l \right)$ and $\left(\sigma_{ij}^l \right)^2 = 1 - \left(\mu_{ij}^l \right)^2$, respectively. Given that the width of layer is large, the central-limit theorem indicates that the preactivation z_j^{l+1} follows a Gaussian distribution $\mathcal{N}(z | m_j^{l+1}; v_j^{l+1})$, where the mean and variance are given below,

$$\begin{aligned} m_j^{l+1} &= \langle z_j^l \rangle = \frac{1}{\sqrt{N_l}} \sum_j \mu_{ij}^l h_i^l \\ \left(v_j^{l+1} \right)^2 &= \langle \left(z_j^{l+1} \right)^2 \rangle - \langle z_j^{l+1} \rangle^2 = \frac{1}{N_l} \sum_j \left(\sigma_{ij}^l \right)^2 \left(h_i^l \right)^2. \end{aligned} \quad (30)$$

Therefore we write the preactivation as $z_i^l = m_i^l + \epsilon_i^l v_i^l$, where ϵ_i^l denotes a standard Gaussian variable relying on the layer and weight-component index. Then, we can compute the gradients as follows,

$$\frac{\partial \mathcal{L}_{rec}}{\partial \theta_{ij}^l} = \frac{\partial \mathcal{L}_{rec}}{\partial z_j^{l+1}} \frac{\partial z_j^{l+1}}{\partial \theta_{ij}^l} = \mathcal{K}_j^{l+1} \left(\frac{\partial m_j^{l+1}}{\partial \theta_{ij}^l} + \epsilon_j^{l+1} \frac{\partial v_j^{l+1}}{\partial \theta_{ij}^l} \right), \quad (31)$$

where we have defined $\mathcal{K}_j^{l+1} = \frac{\partial \mathcal{L}_{rec}}{\partial z_j^{l+1}}$, which could be solved using the chain rule. The term $\frac{\partial m_j^{l+1}}{\partial \theta_{ij}^l}$ and $\frac{\partial v_j^{l+1}}{\partial \theta_{ij}^l}$ can be directly derived from Eq.(30), as shown below,

$$\begin{aligned}\frac{\partial m_j^{l+1}}{\partial \theta_{ij}^l} &= \frac{1}{\sqrt{N_l}} \beta h_i^l (\sigma_{ij}^l)^2, \\ \frac{\partial v_j^{l+1}}{\partial \theta_{ij}^l} &= -\beta \frac{(h_i^l)^2}{N_l v_j^{l+1}} \mu_{ij}^l (\sigma_{ij}^l)^2,\end{aligned}\tag{32}$$

and \mathcal{K}_i^l can be estimated by the chain rule from the value at the top layer, i.e.,

$$\mathcal{K}_i^l = \sum_j \mathcal{K}_j^{l+1} \left(\frac{1}{\sqrt{N_l}} \mu_{ij}^l + \frac{\epsilon_j^{l+1}}{N_l \sqrt{(v_j^{l+1})^2}} (\sigma_{ij}^l)^2 h_i^l \right) f'(z_i^l),\tag{33}$$

where $f'(\cdot)$ is the derivative of transfer function, and on the top layer, \mathcal{K}_i^L can be directly estimated as $\mathcal{K}_i^L = -\hat{h}_i(1 - h_i^L)$. Taken together, the total gradients on the loss function \mathcal{L} take the form as

$$\frac{\partial \mathcal{L}}{\partial \theta_{ij}^{l,k}} = \beta \left(\sigma_{ij}^{l,k} \right)^2 \left(\beta \Delta_{ij}^{l,k} + \delta_{ij}^{l,k} \right),\tag{34}$$

where we add the step index k as $\delta_{ij}^{l,k} = \mathcal{K}_j^{l+1} \left(\frac{1}{\sqrt{N_l}} h_i^l - \frac{\epsilon_j^{l+1}}{N_l v_j^{l+1}} (h_i^l)^2 \mu_{ij}^l \right)$. It can be clearly seen that the variance of w_{ij}^l at the iteration step k together with the inverse temperature $\beta \left(\sigma_{ij}^{l,k} \right)^2$ tunes the learning rate η , where a larger variance leads to larger gradients in the iteration step k . In addition, the regularization term $\beta \Delta_{ij}^{l,k-1}$ measures the similarity between the variational posterior probabilities across successive learning steps, which regulates the distance from current guess to previous one, providing a principled way to use the information from previous task knowledges. Therefore, this variational continual learning can be used in scenarios where task boundaries are not available [13], which is also more cognitively plausible from our humans' learning experiences. Hereafter, we call this variational continual learning scheme as VCL.

We emphasize the relationship between the VCL used in toy model analysis in previous section and that used for practical continual deep learning in this section. In essence, the VCL in these two sections bears the same principle [see Eq. (26)]. In the toy model analysis, we specify the task boundary, which allows us to derive the Franz-Parisi potential of the continual learning. However, in a practical training, a task agnostic training is favored (like

humans), which is exactly captured in Eq. (34). Therefore, the last training step acts as a reference in the language of the Franz-Parisi framework, i.e., the learning of the next step can be described by an equilibrium system with an anchored external preference. Furthermore, in the toy model analysis, we set the hyperparameter β for both tasks the same value. In the practical deep learning, β is allowed to increase with epoch [one example is shown in Fig. 7 (a)].

In particular, our learning protocol emphasizes how synaptic uncertainty tunes the continual learning, and thus provides a principled way to understand engineering heuristics [15, 16] and neuroscience inspired heuristics [6, 8, 9]. For the deep networks with binary weights, the previous work uses discretization operation of a continuous weight, surrogate gradient and a metaplasticity function (see details in Appendix A), while our VCL does not require these tricks. In addition, other heuristic strategies such as elastic weight consolidation and its variants [9] can be also unified in our current framework. For example, the part \mathcal{L}_{reg} can be approximated by a term involving the Fisher information matrix as

$$F(\boldsymbol{\theta}) = \mathbb{E}_{q_{\boldsymbol{\theta}}(\mathbf{w})} \left(\left(\frac{\partial \ln q_{\boldsymbol{\theta}}(\mathbf{w})}{\partial \boldsymbol{\theta}} \right) \left(\frac{\partial \ln q_{\boldsymbol{\theta}}(\mathbf{w})}{\partial \boldsymbol{\theta}} \right)^{\top} \right). \quad (35)$$

and then

$$\mathcal{L}_{reg} \approx \frac{1}{2} (\boldsymbol{\theta}^k - \boldsymbol{\theta}^{k-1})^{\top} F(\boldsymbol{\theta}^{k-1}) (\boldsymbol{\theta}^k - \boldsymbol{\theta}^{k-1}), \quad (36)$$

where we take only the diagonal elements of the Fisher information matrix $F(\boldsymbol{\theta}^{k-1}) \approx \beta^2(\boldsymbol{\sigma}^{k-1})^2$, recovering the elastic weight consolidation algorithm. The technical proof is given in appendix B.

B. Learning performance and roles of synaptic uncertainty

In this section, we compare the performance of VCL and the metaplasticity algorithm for neural networks with binary weights. Algorithmic details are given in appendix A. We consider two tasks first— sequential learning of MNIST and Fashion-MNIST (f-MNIST) datasets [8], and this setting requires the network to sequentially learn from two datasets: MNIST and f-MNIST. We next consider a popular continual learning benchmark, namely the permuted MNIST learning task [9]. The permuted MNIST learning task is composed

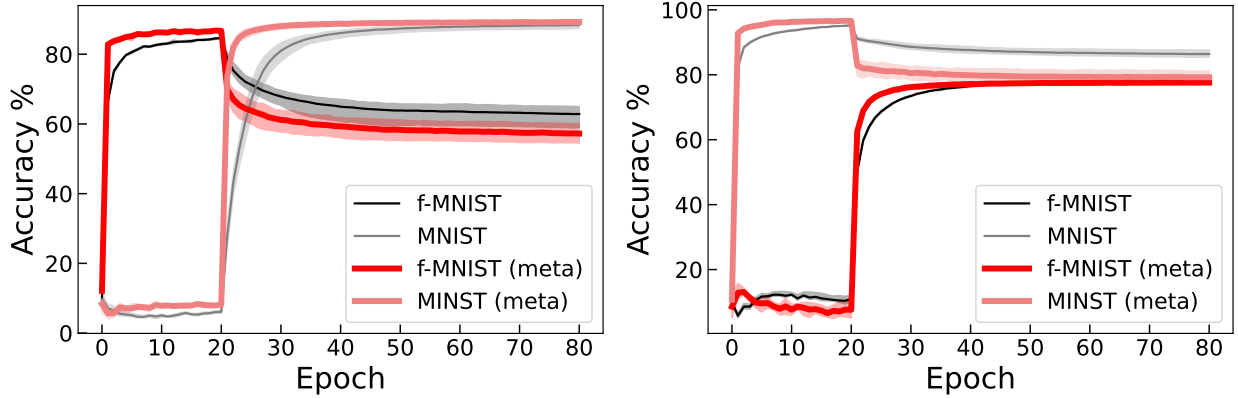


FIG. 6: Continual learning on MNIST and Fashion-MNIST (f-MNIST) datasets. The network has the architecture $[784, 400, 200, 10]$, each number indicates the layer width. The results are averaged over five independent trials. (Left panel) The training order is f-MNIST first and then MNIST. $\beta_1 = 1$ for the first task and $\beta_2 = 12.5$ for the second one in the VCL setting. $m_1 = 0.5$ for the first task and $m_2 = 0.9$ for the second in the metaplasticity algorithm. (Right panel) MNIST is applied first followed by the f-MNIST dataset. The same network architecture is used as (a), while $\beta_1 = 1$, $\beta_2 = 17.5$, $m_1 = 0.5$ and $m_2 = 0.7$.

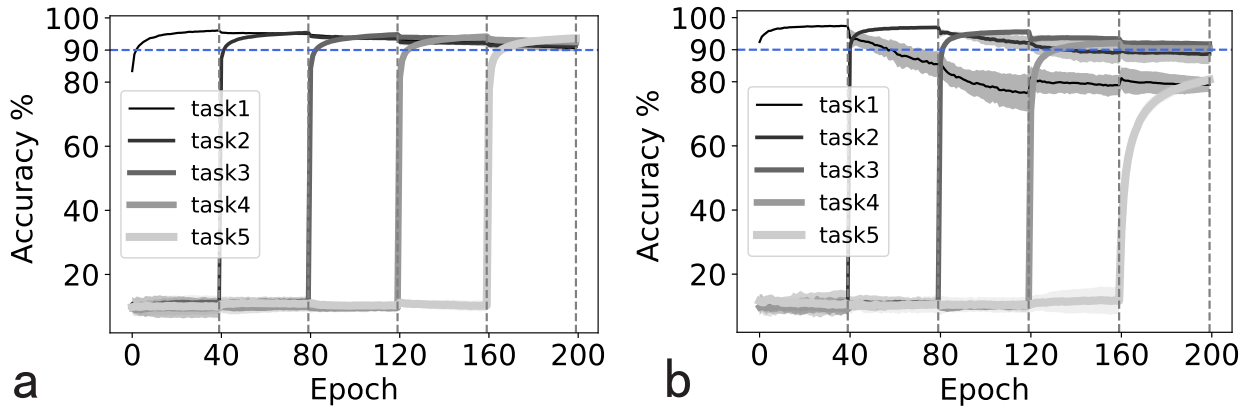


FIG. 7: Continual learning of permuted MNIST learning tasks. Five sequential tasks are considered, and each is trained for 40 epochs. The network has the architecture $[784, 512, 512, 10]$, each number indicates the layer width. The results are averaged over five independent trials. (a) Test accuracy based on VCL, $\beta_\ell = a \tanh(\delta + b\ell/M)$, where ℓ denotes the epoch index, and M is the total number of epochs. We use $a = 10.0$, $\delta = 0.1$, and $b = 2.0$. (b) Test accuracy of the metaplasticity algorithm, for which $m = 0.43$ for all the tasks.

of continual learning of several datasets, and each task contains labeled images of a fixed random spatial permutation of pixels.

Figure 6 shows that for both training orders (f-MNIST first or MNIST first), VCL achieves a much better performance than that of the metaplasticity algorithm (a shorthand as meta), showing the benefit of less forgetting of learned tasks and thus better performance for new coming tasks. The same phenomenon can be also observed in Fig. 7, where five permuted

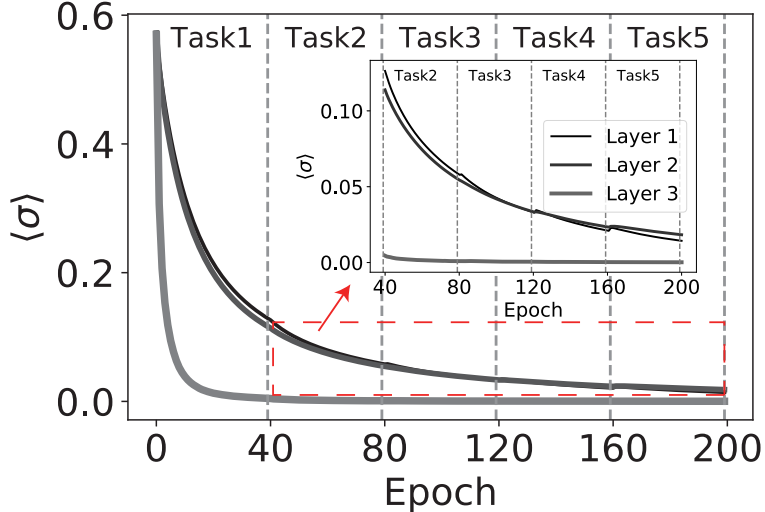


FIG. 8: The averaged level of synaptic uncertainty ($\langle \sigma \rangle$) evolves through training for all the layers, and the inset shows the details of the training stage after 40 epochs. The network architecture is the same as that of Fig. 7.

MNIST datasets are sequentially presented to the network. Networks trained with VCL [Fig. 7 (a)] are learning better and forgetting less previous task knowledge compared with those trained with meta [Fig. 7 (b)]. The plot shows the classification accuracy for task t after learning tasks $t' \geq t$. A perfect continual learning must provide high accuracy for task t , and moreover preserve the performance even when subsequent tasks are learned, which is independent of the training time of each task (e.g., increasing the training time to 100 epochs).

We also plot the evolution of synaptic uncertainty by calculating the average $\langle \sigma \rangle = \frac{1}{\#weights} \sum_{(ij)} \sigma_{ij}^2$ for every epoch and every layer. As expected, the mean uncertainty decreases during the continual learning. However, the level rises with a minor magnitude after a task switch, but then drops again. In addition, the reduction of the uncertainty is also evident for upstream layers, indicating that these layers tend to freeze most of weights, or make them less plastic. In contrast, the last layer maintain a low level of synaptic uncertainty for reading out the key category information. We also observe that the synaptic plasticity with a larger uncertainty has a larger contribution to how strong the KL divergence should change, which thereby plays an important role in minimizing the overall objective. To conclude, the synaptic variance is a key quantity determining the behavior of continual learning. The VCL can adjust the synaptic resources during sequentially learning of multiple tasks.

IV. CONCLUSION

In this study, we focus on the continual learning in deep (or shallow) neural networks with binary weights. Recent works already argued that the variational training is effective in neural networks of real-valued weights [13–15], and a brain-inspired metaplasticity method is also effective in training binary neural networks [8]. However, how to unify these diverse strategies within a statistical physics model is challenging. Here, we propose a variational mean-field framework to incorporate synaptic uncertainty, task-knowledge transfer and mean-field potential for multi-task learning. First, we argue that the synaptic uncertainty plays a key role in modulating continual learning performance, through the lens of variational weight distribution. Specifically, the synaptic variance becomes a modulating factor in the synaptic plasticity rules, based on our theory. Second, the task-knowledge transfer can be interpreted in physics. The knowledge from the previous task behaves as a reference configuration in the Franz-Parisi potential formula [22, 23], an anchor for learning new knowledge. The learning of new task can thus be described by an equilibrium system with an anchored external preference. The derived theory matches well the numerical simulations using stochastic gradient descent algorithms.

Our theory of variational continual learning also predicts that a single-task learning exhibits a continuous transition with increasing amount of data (sample complexity), which is in stark contrast to the previous findings in mean-field theory of generalization (in the direct discrete or continuous weight space) [26, 27]. This new theoretical prediction suggests that the current variational continual learning proves efficient in practical learning, since a trapping by metastable states is absent. We remark that this absence of a first-order transition holds only for shallow networks. It is thus interesting to extend our theoretical analysis to multi-layered networks to see if this conclusion is present or not.

We finally demonstrate that our framework can be applied to continual learning of real datasets, achieving similar or even better performances with those obtained by heuristic strategies, such as metaplasticity. Therefore, this work can be a promising starting point to explore further the important yet challenging question of how to build theoretically-grounded neural representation that helps an intelligent agent avoid catastrophic forgetting and adapt continuously to new tasks, based on accumulated knowledges from previous tasks.

Appendix A: Algorithmic details

In this section, we provide the details of metaplasticity algorithm and VCL, which are compared in the main text. The pseudocode of the metaplasticity algorithm [8] is summarized in Algorithm 1.

Algorithm 1 Metaplasticity continual learning

- 1: Input: h_j^{l-1} , $w_{ij}^l = \text{sign}(a_{ij}^l)$; meta parameter m ; learning rate η
 - 2: Feedforward propagation: $z_i^l = \frac{1}{\sqrt{N^{l-1}}} \sum_j w_{ji}^l h_j^{l-1}$, $h_i^l = f(z_i^l)$, $f(x) = \text{ReLU}(x)$;
 - 3: Backpropagation: $\frac{\partial \mathcal{L}}{\partial w_{ij}^l} = \frac{\partial \mathcal{L}}{\partial z_j^l} \frac{\partial z_j^l}{\partial w_{ij}^l} = \left(\frac{1}{\sqrt{N^{l-1}}} \right) \sum_k \frac{\partial \mathcal{L}}{\partial z_k^{l+1}} w_{jk}^{l+1} f'(z_j^l) h_i^{l-1}$;
 - 4: Parameter update: $(a_{ij}^l)^{k+1} - (a_{ij}^l)^k = -\eta \left(1 - \zeta \tanh^2(m (a_{ij}^l)^k) \right) \frac{\partial \mathcal{L}}{\partial w_{ij}^l}$, where $\zeta = \frac{1}{2} \left[\text{sign} \left(w_{ij}^l \frac{\partial \mathcal{L}}{\partial w_{ij}^l} \right) + 1 \right]$.
-

In the meta algorithm, \mathcal{L} denotes the loss function, and a_{ij}^l denotes the latent real-valued weights underlying binary counterpart, and the core idea is the introduction of a modulation function $f_{\text{meta}}(m, x) = 1 - \tanh^2(mx)$ which is a decreasing function of $|x|$ (or the absolute value of the hidden weights). This modulation called metaplasticity makes the hidden weight change less likely if the corresponding magnitude are growing (consolidation of some useful information, expressed as the ζ factor). Therefore, this metaplasticity can be heuristically thought of as a sort of weight consolidation. In contrast, our VCL gives rise to an alternative modulation related to the synaptic uncertainty, thereby bearing a more solid theoretical ground. In addition, the gradient with respect to a discrete weight value in the meta algorithm is ill-defined, which does not appear in our VCL. We remark that this algorithm is sensitive to the network size; if the size of network is not big enough, this algorithm may fail to give satisfied learning performance.

Our VCL algorithm is summarized in the pseudocode 2. In the main text, we use learning rate—0.01 and mini-batch size—64 for both tasks. Note that the mean and variance of the preactivation \mathbf{z} is computed for each single data sample, given the statistics of the weight. All codes to reproduce our results in the main text are available at the Github link [32].

Algorithm 2 VCL algorithm

- 1: Input: single sample $\mathbf{x} \in \mathbb{R}^{N_0}$, $\mathbf{w}^l \in \mathbb{R}^{N_l \times N_{l+1}}$ from the distribution $q_{\theta_{ij}^l}(w_{ij}^l) = \frac{e^{\beta w_{ij}^l \theta_{ij}^l}}{e^{\beta \theta_{ij}^l} + e^{-\beta \theta_{ij}^l}}$;
 - 2: Compute the mean and variance of elements $\mathbf{w}^l : \boldsymbol{\mu}^l, (\boldsymbol{\sigma}^l)^2$;
 - 3: Compute the mean \mathbf{m}^l and variance $(\mathbf{v}^l)^2$ of preactivation $\mathbf{z}^l = \frac{1}{\sqrt{N_l}}(\mathbf{w}^{l-1})^\top \mathbf{h}^{l-1}$, $\mathbf{h}^0 = \mathbf{x}$;
 - 4: Sample $\boldsymbol{\epsilon}^l \in \mathbb{R}^{N_l}$ independently from $\mathcal{N} \sim (0, 1)$;
 - 5: Output: $\mathbf{z}^l = (\mathbf{m}^l + \boldsymbol{\epsilon}^l \odot \mathbf{v}^l)$, $\mathbf{h}^l = f(\mathbf{z}^l)$;
 - 6: Parameter update: $\theta_{ij}^{l,k+1} = \theta_{ij}^{l,k} - \eta \frac{\partial \mathcal{L}}{\partial \theta_{ij}^{l,k}}$, where $\frac{\partial \mathcal{L}}{\partial \theta_{ij}^{l,k}} = \beta \left(\sigma_{ij}^{l,k} \right)^2 \left(\beta \Delta_{ij}^{l,k-1} + \mathcal{K}_j^{l+1} \left(\frac{1}{\sqrt{N_l}} h_i^l - \frac{\epsilon_j^{l+1}}{N_l v_j^{l+1}} (h_i^l)^2 \mu_{ij}^l \right) \right)$, and $\Delta_{ij}^{l,k-1} = \theta_{ij}^{l,k-1} - \theta_{ij}^{l,k-2}$.
-

Appendix B: Connection to elastic weight consolidation

In this section, we provide a proof of the elastic weight consolidation as a special example of VCL. We first write $D(\boldsymbol{\theta}^k, \boldsymbol{\theta}^{k-1}) \equiv \mathcal{L}_{reg} = \text{KL}[q_{\boldsymbol{\theta}^k}(\mathbf{w}) \| q_{\boldsymbol{\theta}^{k-1}}(\mathbf{w})]$, and then we have

$$D(\boldsymbol{\theta}^k, \boldsymbol{\theta}^{k-1}) = \int q(\mathbf{w}; \boldsymbol{\theta}^k) \ln \frac{q(\mathbf{w}; \boldsymbol{\theta}^k)}{q(\mathbf{w}; \boldsymbol{\theta}^{k-1})} d\mathbf{w}, \quad (\text{B1})$$

where the integral can be interpreted as the summation for the considered discrete weight variable. Hereafter, we write $q_{\boldsymbol{\theta}^k}(\mathbf{w}) = q(\mathbf{w}; \boldsymbol{\theta}^k)$. We next assume the two consecutive solutions are sufficiently close, i.e., $\boldsymbol{\theta}^k \approx \boldsymbol{\theta}^{k-1}$, or $\boldsymbol{\theta}^k = \boldsymbol{\theta}^{k-1} + \Delta \boldsymbol{\theta}$ ($\Delta \boldsymbol{\theta} \rightarrow 0$), and then we consider alternatively $D(\boldsymbol{\theta}^{k-1}, \boldsymbol{\theta}^k)$ because of small $\Delta \boldsymbol{\theta}$, and further expand $\ln q(\mathbf{w}; \boldsymbol{\theta}^k)$ around $\boldsymbol{\theta}^{k-1}$ up to the second order,

$$\begin{aligned} D(\boldsymbol{\theta}^{k-1}, \boldsymbol{\theta}^k) &= \mathbb{E}_{q(\mathbf{w}; \boldsymbol{\theta}^{k-1})} [\ln q(\mathbf{w}; \boldsymbol{\theta}^{k-1}) - \ln q(\mathbf{w}; \boldsymbol{\theta}^k)], \\ &\approx -(\boldsymbol{\theta}^k - \boldsymbol{\theta}^{k-1})^\top \mathbb{E}_{q(\mathbf{w}; \boldsymbol{\theta}^{k-1})} \left(\frac{\partial \ln q(\mathbf{w}; \boldsymbol{\theta}^{k-1})}{\partial \boldsymbol{\theta}^{k-1}} \right) \\ &\quad - \frac{1}{2} (\boldsymbol{\theta}^k - \boldsymbol{\theta}^{k-1})^\top \mathbb{E}_{q(\mathbf{w}; \boldsymbol{\theta}^{k-1})} \left(\frac{\partial^2}{\partial (\boldsymbol{\theta}^{k-1})^2} \ln q(\mathbf{w}; \boldsymbol{\theta}^{k-1}) \right) (\boldsymbol{\theta}^k - \boldsymbol{\theta}^{k-1}). \end{aligned} \quad (\text{B2})$$

We also find that

$$\begin{aligned}
\mathbb{E}_{q(\mathbf{w}; \boldsymbol{\theta}^{k-1})} \frac{\partial \ln q(\mathbf{w}; \boldsymbol{\theta}^{k-1})}{\partial \boldsymbol{\theta}^{k-1}} &= \int q(\mathbf{w}; \boldsymbol{\theta}^{k-1}) \frac{1}{q(\mathbf{w}; \boldsymbol{\theta}^{k-1})} \frac{\partial q(\mathbf{w}; \boldsymbol{\theta}^{k-1})}{\partial \boldsymbol{\theta}^{k-1}} d\mathbf{w}, \\
&= \frac{\partial}{\partial \boldsymbol{\theta}^{k-1}} \int q(\mathbf{w}; \boldsymbol{\theta}^{k-1}) d\mathbf{w}, \\
&= \frac{\partial 1}{\partial \boldsymbol{\theta}^{k-1}} = 0.
\end{aligned} \tag{B3}$$

Notice that $\mathbb{E}_q \left(\frac{\partial^2 \ln q}{\partial (\boldsymbol{\theta}^{k-1})^2} \right) = \mathbb{E}_q \left(\frac{1}{q} \frac{\partial^2 q}{\partial (\boldsymbol{\theta}^{k-1})^2} - \left(\frac{\partial \ln q}{\partial \boldsymbol{\theta}^{k-1}} \right)^2 \right)$, where q represents $q(\mathbf{w}; \boldsymbol{\theta}^{k-1})$, and we have used $\frac{\partial^2 \int d\mathbf{w} q}{\partial (\boldsymbol{\theta}^{k-1})^2} = 0$, we finally arrive at

$$D(\boldsymbol{\theta}^k, \boldsymbol{\theta}^{k-1}) = \frac{1}{2} (\boldsymbol{\theta}^k - \boldsymbol{\theta}^{k-1})^\top F(\boldsymbol{\theta}) (\boldsymbol{\theta}^k - \boldsymbol{\theta}^{k-1}), \tag{B4}$$

where $D(\boldsymbol{\theta}^k, \boldsymbol{\theta}^{k-1}) \simeq D(\boldsymbol{\theta}^{k-1}, \boldsymbol{\theta}^k)$ when $\Delta \boldsymbol{\theta} \rightarrow 0$, and $F(\boldsymbol{\theta})$ is exactly the Fisher information matrix whose definition is given by $F(\boldsymbol{\theta}) = \mathbb{E}_{q(\mathbf{w}; \boldsymbol{\theta}^{k-1})} \left[\left(\frac{\partial}{\partial \boldsymbol{\theta}^{k-1}} \ln q(\mathbf{w}; \boldsymbol{\theta}^{k-1}) \right) \left(\frac{\partial}{\partial \boldsymbol{\theta}^{k-1}} \ln q(\mathbf{w}; \boldsymbol{\theta}^{k-1}) \right)^\top \right]$. To conclude, when we take only the diagonal elements of the Fisher information matrix, we recover the elastic weight consolidation algorithm [9].

Appendix C: Details for replica computation

In this section, we demonstrate how to predict the generalization errors of variational continual learning by replica computation. First, we summarize our problem settings: we consider a teacher-student continual learning problem on binary perceptron, where the student learns task 1 first and then task 2. For the data in these two tasks \mathbf{x}^1 and \mathbf{x}^2 , the labels are given by two teachers, $y^1 = \text{sign}(\sum_i W_i^1 x_i^1)$ and $y^2 = \text{sign}(\sum_i W_i^2 x_i^2)$. Note that, each dimension of the input data follows a uniform Bernoulli distribution, $x_i^{t,\mu} \in [-1, +1]$ and the training datasets of the two tasks consider different realizations, $\mathcal{D}_t = \{\mathbf{x}^{t,\mu}, y^{t,\mu}\}_{\mu=1}^{M_t}$, where $t = 1, 2$. There is also a correlation between these two teachers, described by an overlap $r_0 = \frac{1}{N} \sum_i W_i^1 W_i^2$. Therefore, the joint distribution of teachers' weights can be

parameterized as,

$$P_0(W_i^1, W_i^2) = \frac{1+r_0}{4}\delta(W_i^1 - W_i^2) + \frac{1-r_0}{4}\delta(W_i^1 + W_i^2), \quad (\text{C1})$$

where we use the notation—teacher-average to denote the average over such distribution. For the sake of convenience, we assume that during the learning of a certain task, the loss function is fixed. According to the variational theory in the main text, the loss functions for the continual learning are listed as follows,

$$\begin{aligned} \mathcal{L}_1(\mathbf{m}) &= -\sum_{\mu=1}^{M_1} \ln H \left(-\frac{\text{sign}(\sum_i W_i^1 x_i^{1,\mu}) \sum_i m_i x_i^{1,\mu}}{\sqrt{\sum_i (1-m_i^2)}} \right), \\ \mathcal{L}_2(\mathbf{m}) &= -\sum_{\mu=1}^{M_2} \ln H \left(-\frac{\text{sign}(\sum_i W_i^1 x_i^{2,\mu}) \sum_i m_i x_i^{2,\mu}}{\sqrt{\sum_i (1-m_i^2)}} \right) + \sum_{i=1}^N \text{KL}(Q_{m_i} \| Q_{m_{1,i}}). \end{aligned} \quad (\text{C2})$$

where $H(x) = \frac{1}{2}\text{erfc}\left(\frac{x}{\sqrt{2}}\right)$ and \mathbf{m}_1 is the trained weight after learning task 1. In the following, the learning procedures of task 1 and task 2 will be called as single-task learning and multi-task learning respectively, which actually reflects the learning's essence.

To predict the generalization errors in both learning scenarios, we apply replica method under the replica symmetry Ansatz. For a specific learning scenario, the derivations can be unfolded in two steps: First, we treat the loss function for gradient-descent training as the Hamiltonian in canonical ensemble and compute its averaged free energy, which entails the replica trick; Second, with the knowledge of the free energy, we show how to obtain the generalization errors of both tasks. In the following, the value of M can be M_1 or M_2 depending on the learning stage.

1. Thermodynamic system for single-task learning

In this scenario, the thermodynamic system can be defined by a partition function,

$$Z = \int_{\Omega} \prod_{i=1}^N dm_i e^{-\beta \mathcal{L}_1(\mathbf{m})} = \int_{\Omega^N} \prod_{i=1}^N dm_i \prod_{\mu=1}^{M_1} H^{\beta} \left(-\frac{\text{sign}(\sum_i W_i^1 x_i^{1,\mu}) \sum_i m_i x_i^{1,\mu}}{\sqrt{\sum_i (1-m_i^2)}} \right), \quad (\text{C3})$$

where $\Omega = [-1, +1]$. Our goal is to compute the quenched average of the free energy $\langle \ln Z \rangle$ over the dataset \mathcal{D}_1 and teacher average. We can first remove the average over $P(\mathbf{W}^1)$ by

performing a gauge transformation: $x_i^{1,\mu} \rightarrow W_i^1 x_i^{1,\mu}$, $m_i \rightarrow W_i^1 m_i$. The result can be seen as setting $W_i^1 = 1, \forall i$. Then, we apply replica trick, $\langle \ln Z \rangle = \lim_{n \rightarrow \infty} \frac{\ln \langle Z^n \rangle}{n}$, which requires to compute the replicated partition function,

$$\langle Z^n \rangle = \int_{\Omega^{nN}} \prod_{a=1}^n \prod_{i=1}^N dm_i^a \left\langle \prod_{a=1}^n \prod_{\mu=1}^{M_1} H^\beta \left(-\frac{\text{sign}(\sum_i W_i^1 x_i^{1,\mu}) \sum_i m_i^a x_i^{1,\mu}}{\sqrt{\sum_i 1 - (m_i^a)^2}} \right) \right\rangle. \quad (\text{C4})$$

Now, we introduce the local field,

$$u^a = \frac{\sum_i m_i^a x_i^1}{\sqrt{N}}, \quad v_1 = \frac{\sum_i W_i^1 x_i^1}{\sqrt{N}}, \quad (\text{C5})$$

where the data index μ is omitted in advance. Note that, the statistics of local fields stem from the data distribution. According to central limit theorem, local fields should obey joint Gaussian distribution in the thermodynamics limit $N \rightarrow \infty$. Thus, we have the following statistics

$$\langle u^a \rangle = 0, \quad \langle v_1 \rangle = 0. \quad (\text{C6})$$

In addition,

$$\begin{aligned} \langle u^a u^a \rangle - \langle u^a \rangle \langle u^a \rangle &= \frac{\sum_i m_i^a m_i^a}{N}, \\ \langle u^a u^b \rangle - \langle u^a \rangle \langle u^b \rangle &= \frac{\sum_i m_i^a m_i^b}{N}, \\ \langle v_1 u^a \rangle - \langle v_1 \rangle \langle u^a \rangle &= \frac{\sum_i W_i^1 m_i^a}{N}, \end{aligned} \quad (\text{C7})$$

where order parameters $q_{ab} = \frac{\sum_i m_i^a m_i^b}{N}$, $q_{aa} = \frac{\sum_i m_i^a m_i^a}{N}$, $r_a^1 = \frac{\sum_i W_i^1 m_i^a}{N}$ naturally appear. We enforce the definitions of these order parameters to the replicated partition function by the Fourier Integral of Dirac delta functions,

$$\begin{aligned} \delta \left(\sum_i m_i^a m_i^b - q_{ab} N \right) &= \int \frac{1}{2\pi i} e^{\hat{q}_{ab} (\sum_i m_i^a m_i^b - q_{ab} N)} d\hat{q}_{ab}, \\ \delta \left(\sum_i m_i^a m_i^a - q_{aa} N \right) &= \int \frac{1}{4\pi i} e^{\frac{1}{2} \hat{q}_{aa} (\sum_i m_i^a m_i^a - q_{aa} N)} d\hat{q}_{aa}, \\ \delta \left(\sum_i W_i^1 m_i^a - r_a^1 N \right) &= \int \frac{1}{2\pi i} e^{\hat{r}_a^1 (\sum_i W_i^1 m_i^a - r_a^1 N)} d\hat{r}_a^1, \end{aligned} \quad (\text{C8})$$

and then we obtain,

$$\begin{aligned}
\langle Z^n \rangle &= \int \prod_a \frac{d\hat{r}_a^1 dr_a^1}{2\pi i/N} \prod_a \frac{d\hat{q}_{aa} dq_{aa}}{4\pi i/N} \prod_{a<b} \frac{d\hat{q}_{ab} dq_{ab}}{2\pi i/N} e^{-N \sum_{a<b} \hat{q}_{ab} q_{ab} - \frac{1}{2}N \sum_a \hat{q}_{aa} q_{aa} - N \sum_a \hat{r}_a^1 r_a^1} \\
&\int_{\Omega^n} \prod_{a=1}^n \prod_{i=1}^N dm_i^a e^{\sum_{a<b} \hat{q}_{ab} \sum_i m_i^a m_i^b + \frac{1}{2} \sum_a \hat{q}_{aa} \sum_i m_i^a m_i^a} e^{\sum_a \hat{r}_a^1 \sum_i m_i^a} \left\langle \prod_{\mu=1}^{M_1} \prod_{a=1}^n H^\beta \left(-\frac{\text{sign}(v_1) u^a}{\sqrt{1 - q_{aa}}} \right) \right\rangle
\end{aligned} \tag{C9}$$

Note that we introduce a prefactor $1/\sqrt{N}$ in the summations in Eq. (C3), which does not affect the result. Here, we consider the replica symmetry Ansatz: $q_{ab} = q_0$, $\hat{q}_{ab} = \hat{q}_0$, $q_{aa} = q_d$, $\hat{q}_{aa} = \hat{q}_d$, $r_a^1 = r_1$, $\hat{r}_a^1 = \hat{r}_1$. Next, we will define and compute three terms separately and put them together in the final expression of the free energy:

The first term is the interaction term G_I ,

$$\begin{aligned}
G_I &= -\frac{1}{2} \sum_{a,b} \hat{q}_{ab} q_{ab} - \sum_a \hat{r}_a^1 r_a^1 \\
&= -\frac{1}{2} \left(\sum_a \hat{q}_{aa} q_{aa} + \sum_{a \neq b} \hat{q}_{ab} q_{ab} \right) - n \hat{r}_1 r_1 \\
&= -\frac{1}{2} (n \hat{q}_d q_d + n(n-1) \hat{q}_0 q_0) - n \hat{r}_1 r_1.
\end{aligned} \tag{C10}$$

The second contribution is the entropy term G_S ,

$$\begin{aligned}
G_S &= \int_{[-1,1]^n} \prod_a dm_a e^{\frac{1}{2} \sum_{ab} \hat{q}_{ab} m_a m_b + \hat{r}_1 \sum_a m_a}, \\
&= \int_{[-1,1]^n} \prod_a dm_a e^{\frac{1}{2} \hat{q}_d \sum_a m_a m_a - \frac{1}{2} \hat{q}_0 \sum_a m_a m_a + \frac{1}{2} \hat{q}_0 (\sum_a m_a)^2 + \hat{r}_1 \sum_a m_a}, \\
&= \int_{[-1,1]^n} \prod_a dm_a e^{\frac{1}{2} \hat{q}_d \sum_a m_a m_a - \frac{1}{2} \hat{q}_0 \sum_a m_a m_a + \hat{r}_1 \sum_a m_a} \int \mathcal{D}z e^{\sqrt{\hat{q}_0} \sum_a m_a z}, \\
&= \int \mathcal{D}z \left(\int_{-1}^{+1} dm e^{\frac{1}{2} \hat{q}_d m^2 - \frac{1}{2} \hat{q}_0 m^2 + \sqrt{\hat{q}_0} m z + \hat{r}_1 m} \right)^n.
\end{aligned} \tag{C11}$$

Finally, we compute the energy term G_E ,

$$G_E = \left\langle \prod_a H^\beta \left(-\frac{\text{sign}(v_1) u^a}{\sqrt{1 - q_d}} \right) \right\rangle, \tag{C12}$$

where $\langle \cdot \rangle$ denotes the average over the joint distribution of the local fields (u^a, v_1) . Based on their statistics, $\langle u^a u^a \rangle = q_d$, $\langle u^a u^b \rangle = q_0$, $\langle v_1 u^a \rangle = r_1$, $\langle v_1 v_1 \rangle = 1$, they can thus be

parametrized as

$$\begin{aligned} u^a &= \sqrt{q_d - q_0} \sigma_a + \sqrt{q_0} z, \\ v_1 &= \frac{r_1}{\sqrt{q_0}} z + \sqrt{1 - \frac{r_1^2}{q_0}} y, \end{aligned} \quad (\text{C13})$$

where σ_a, z, y are all standard Gaussian variables. Substituting Eq. (C13) into the energy term arrives at

$$\begin{aligned} G_E &= \left\langle \prod_a H^\beta \left(-\frac{\text{sign}(v_1) u^a}{\sqrt{1 - q_d}} \right) \right\rangle \\ &= \int \mathcal{D}z \int \mathcal{D}y \prod_a \int \mathcal{D}\sigma_a H^\beta \left(-\frac{\text{sign} \left(\frac{r_1}{\sqrt{q_0}} z + \sqrt{1 - \frac{r_1^2}{q_0}} y \right) (\sqrt{q_d - q_0} \sigma_a + \sqrt{q_0} z)}{\sqrt{1 - q_d}} \right) \\ &= \int \mathcal{D}z \int \mathcal{D}y \left(\int \mathcal{D}\sigma H^\beta \left(-\frac{\text{sign} \left(\frac{r_1}{\sqrt{q_0}} z + \sqrt{1 - \frac{r_1^2}{q_0}} y \right) (\sqrt{q_d - q_0} \sigma + \sqrt{q_0} z)}{\sqrt{1 - q_d}} \right) \right)^n \\ &= \int \mathcal{D}z \left[H \left(-\frac{r_1}{\sqrt{q_0 - r_1^2}} z \right) \left(\int \mathcal{D}\sigma H^\beta \left(-\frac{\sqrt{q_d - q_0} \sigma + \sqrt{q_0} z}{\sqrt{1 - q_d}} \right) \right)^n + \right. \\ &\quad \left. \left(1 - H \left(-\frac{r_1}{\sqrt{q_0 - r_1^2}} z \right) \right) \left(\int \mathcal{D}\sigma H^\beta \left(\frac{\sqrt{q_d - q_0} \sigma + \sqrt{q_0} z}{\sqrt{1 - q_d}} \right) \right)^n \right] \\ &= \int \mathcal{D}z 2H \left(-\frac{r_1}{\sqrt{q_0 - r_1^2}} z \right) \left(\int \mathcal{D}\sigma H^\beta \left(-\frac{\sqrt{q_d - q_0} \sigma + \sqrt{q_0} z}{\sqrt{1 - q_d}} \right) \right)^n. \end{aligned} \quad (\text{C14})$$

Note that $\mathcal{D}z$ indicates the standard Gaussian measure.

Finally, under the replica symmetry Ansatz, the replicated partition function can be written as

$$\langle Z^n \rangle = \int \prod_a \frac{d\hat{r}_a^1 d\hat{r}_a^1}{2\pi i/N} \prod_a \frac{d\hat{q}_{aa} d\hat{q}_{aa}}{4\pi i/N} \prod_{a < b} \frac{d\hat{q}_{ab} d\hat{q}_{ab}}{2\pi i/N} e^{-Nn f_{\text{RS}}}. \quad (\text{C15})$$

Then, under the saddle-point approximation in the large N limit, the free energy density is given by

$$-\beta f_{\text{RS}} = \lim_{n \rightarrow 0, N \rightarrow \infty} \frac{\ln \langle Z^n \rangle}{nN} = \lim_{n \rightarrow 0} -\frac{1}{2} (\hat{q}_d q_d + (n-1) \hat{q}_0 q_0) - \hat{r}_1 r_1 + \frac{\ln G_S}{n} + \alpha_1 \frac{\ln G_E}{n}. \quad (\text{C16})$$

The free energy should be optimized with respect to the order parameters, and thus we have

to derive the corresponding saddle-point equations through setting the gradients zero. We first compute $g_S = \lim_{n \rightarrow 0} \frac{\ln G_S}{n}$ and $g_E = \lim_{n \rightarrow 0} \frac{\ln G_E}{n}$,

$$\begin{aligned}
g_S &= \lim_{n \rightarrow 0} \frac{\ln G_S}{n} = \lim_{n \rightarrow 0} \frac{1}{n} \int \mathcal{D}z \left(\int_{-1}^{+1} dm e^{\frac{1}{2}\hat{q}_d m^2 - \frac{1}{2}\hat{q}_0 m^2 + \sqrt{\hat{q}_0} m z + \hat{r}_1 m} \right)^n \\
&= \int \mathcal{D}z \ln \left(\int_{-1}^{+1} dm e^{\frac{1}{2}\hat{q}_d m^2 - \frac{1}{2}\hat{q}_0 m^2 + \sqrt{\hat{q}_0} m z + \hat{r}_1 m} \right). \\
g_E &= \lim_{n \rightarrow 0} \frac{\ln G_E}{n} = \ln \int \mathcal{D}z 2H \left(-\frac{r_1}{\sqrt{q_0 - r_1^2}} z \right) \left(\int \mathcal{D}\sigma H^\beta \left(-\frac{\sqrt{q_d - q_0}\sigma + \sqrt{q_0}z}{\sqrt{1 - q_d}} \right) \right)^n \\
&= \int \mathcal{D}z 2H \left(-\frac{r_1}{\sqrt{q_0 - r_1^2}} z \right) \ln \int \mathcal{D}\sigma H^\beta \left(-\frac{\sqrt{q_d - q_0}\sigma + \sqrt{q_0}z}{\sqrt{1 - q_d}} \right).
\end{aligned} \tag{C17}$$

Thus, the saddle-point equations can be expressed as,

$$\begin{aligned}
q_d &= 2 \frac{\partial g_S}{\partial \hat{q}_d}, & q_0 &= -2 \frac{\partial g_S}{\partial \hat{q}_0}, & r_1 &= \frac{\partial g_S}{\partial \hat{r}_1}; \\
\hat{q}_d &= 2\alpha_1 \frac{\partial g_E}{\partial q_d}, & \hat{q}_0 &= -2\alpha_1 \frac{\partial g_E}{\partial q_0}, & \hat{r}_1 &= \alpha_1 \frac{\partial g_E}{\partial r_1}.
\end{aligned} \tag{C18}$$

To make the expressions more compact, we define a probability measure,

$$\langle\langle \mathcal{O} \rangle\rangle_{\mathcal{H}(m)} = \frac{\int_{-1}^{+1} \mathcal{O} e^{\mathcal{H}(m)} dm}{\int_{-1}^{+1} e^{\mathcal{H}(m)} dm}. \tag{C19}$$

Then, we have,

$$\begin{aligned}
q_d &= 2 \int \mathcal{D}z \frac{\int_{-1}^{+1} \frac{1}{2} m^2 e^{\mathcal{I}(m,z)} dm}{\int_{-1}^{+1} e^{\mathcal{I}(m,z)} dm} = \int \mathcal{D}z \langle\langle m^2 \rangle\rangle_{\mathcal{I}(m,z)}, \\
q_0 &= -2 \int \mathcal{D}z \frac{\int_{-1}^{+1} \left(-\frac{1}{2} m^2 + \frac{z}{2\sqrt{\hat{q}_0}} m \right) e^{\mathcal{I}(m,z)} dm}{\int_{-1}^{+1} e^{\mathcal{I}(m,z)} dm} = \int \mathcal{D}z \langle\langle m^2 - \frac{z}{\sqrt{\hat{q}_0}} m \rangle\rangle_{\mathcal{I}(m,z)}, \\
r_1 &= \int \mathcal{D}z \frac{\int_{-1}^{+1} m e^{\mathcal{I}(m,z)} dm}{\int_{-1}^{+1} e^{\mathcal{I}(m,z)} dm} = \int \mathcal{D}z \langle\langle m \rangle\rangle_{\mathcal{I}(m,z)},
\end{aligned} \tag{C20}$$

where

$$\mathcal{I}(m, z) = \frac{1}{2}\hat{q}_d m^2 - \frac{1}{2}\hat{q}_0 m^2 + \sqrt{\hat{q}_0} m z + \hat{r}_1 m. \tag{C21}$$

The other derivatives related to g_E can be computed as,

$$\begin{aligned}
\hat{q}_d &= 4\alpha_1 \int \mathcal{D}z H(\lambda(z)) \frac{\int \mathcal{D}\sigma \beta H^{\beta-1}(\gamma(z, \sigma)) H'(\gamma(z, \sigma)) u(z, \sigma)}{\int \mathcal{D}\sigma H^\beta(\gamma(z, \sigma))}, \\
\hat{q}_0 &= -4\alpha_1 \int \mathcal{D}z H'(\lambda(z)) v_1(z) \ln \int \mathcal{D}\sigma H^\beta(\gamma(z, \sigma)) \\
&\quad - 4\alpha_1 \int \mathcal{D}z H(\lambda(z)) \frac{\int \mathcal{D}\sigma \beta H^{\beta-1}(\gamma(z, \sigma)) H'(\gamma(z, \sigma)) w(z, \sigma)}{\int \mathcal{D}\sigma H^\beta(\gamma(z, \sigma))}, \\
\hat{r}_1 &= 2\alpha_1 \int \mathcal{D}z H'(\lambda(z)) h(z) \ln \int \mathcal{D}\sigma H^\beta(\gamma(z, \sigma)),
\end{aligned} \tag{C22}$$

where

$$\begin{aligned}
\lambda(z) &= -\frac{r_1}{\sqrt{q_0 - r_1^2}} z, \\
\gamma(z, \sigma) &= -\frac{\sqrt{q_d - q_0} \sigma + \sqrt{q_0} z}{\sqrt{1 - q_d}}, \\
u(z, \sigma) &= \frac{(q_0 - 1)\sigma - \sqrt{q_0} \sqrt{q_d - q_0} z}{2(1 - q_d)^{\frac{3}{2}} \sqrt{q_d - q_0}}, \\
v_1(z) &= \frac{r_1 z}{2(q_0 - r_1^2)^{\frac{3}{2}}}, \\
w(z, \sigma) &= \frac{\sqrt{q_0} \sigma - \sqrt{q_d - q_0} z}{2\sqrt{1 - q_d} \sqrt{q_d - q_0} \sqrt{q_0}}, \\
h(z) &= \frac{-q_0 z}{(q_0 - r_1^2)^{\frac{3}{2}}}.
\end{aligned} \tag{C23}$$

a. Generalization error for task 1

During the learning of task 1, the generalization error can be defined as

$$\epsilon_g^1 = \left\langle \Theta \left(-\text{sign} \left(\sum_i W_i^1 x_i^* \right) \sum_i \text{sign}(m_i) x_i^* \right) \right\rangle, \tag{C24}$$

where \mathbf{x}^* is one fresh example (or a test data). Note that, the average $\langle \cdot \rangle$ refers to the ensemble average based on the thermodynamic system for task 1. To handle this average, we define similar local fields for test data,

$$u^* = \frac{\sum_i \text{sign}(m_i) x_i^*}{\sqrt{N}}, \quad v_1^* = \frac{\sum_i W_i^1 x_i^*}{\sqrt{N}}, \tag{C25}$$

whose statistical properties are as follows, $\langle v_1^* v_1^* \rangle = 1$, $\langle u^* u^* \rangle = 1$, $p_1 = \langle v_1^* u^* \rangle = \frac{1}{N} \sum_i \text{sign}(m_i) W_i^1$. Then, local fields are parametrized as

$$\begin{aligned} u^* &= z, \\ v_1^* &= p_1 z + \sqrt{1 - p_1^2} y. \end{aligned} \tag{C26}$$

The generalization error becomes

$$\begin{aligned} \epsilon_g^1 &= \int \mathcal{D}z \int \mathcal{D}y \Theta \left(-\text{sign}(p_1 z + \sqrt{1 - p_1^2} y) z \right) \\ &= \int \mathcal{D}z \, 2H \left(-\frac{p_1}{\sqrt{1 - p_1^2}} z \right) \Theta(-z) \\ &= \frac{1}{\pi} \arccos(p_1), \end{aligned} \tag{C27}$$

which introduces a new order parameter p_1 . To obtain the value of p_1 , we should first introduce the order parameter to the original replicated partition function by a Fourier integral representation of the Dirac delta function. After some manipulations, the free energy density under the replica symmetry Ansatz and the limit of $n \rightarrow 0$ is rewritten as

$$-\beta f_{\text{RS}} = -\frac{1}{2} (\hat{q}_d q_d + (n-1) \hat{q}_0 q_0) - \hat{r}_1 r_1 - \hat{p}_1 p_1 + g'_S + \alpha_1 g_E \tag{C28}$$

where the energy term g_E remains the same, but the entropy term g'_S changes as follows,

$$g'_S = \int \mathcal{D}z \ln \left(\int_{-1}^{+1} dm \, e^{\frac{1}{2} \hat{q}_d m^2 - \frac{1}{2} \hat{q}_0 m^2 + \sqrt{\hat{q}_0} m z + \hat{r}_1 m + \hat{p}_1 \text{sign}(m)} \right). \tag{C29}$$

In the new saddle-point equations, it is easy to find that $\hat{p}_1 = \alpha_1 \frac{\partial g_E}{\partial p_1} = 0$, which means the original saddle-point equations [Eqs. (C20), (C22)] are independent of the new order parameters p_1 and \hat{p}_1 . Thus, after the convergence of iterating the original saddle-point equations, we compute p_1 by $p_1 = \frac{\partial g'_S}{\partial \hat{p}_1}$ and obtain the following result as

$$p_1 = \int \mathcal{D}z \langle \langle \text{sign}(m) \rangle \rangle_{\mathcal{I}(m,z)}. \tag{C30}$$

b. *Generalization error for task 2*

The calculation of generalization error for task 2 follows a similar line, except for one important difference, which is the involvement of the teacher-average over the joint distribution $P(\mathbf{W}^1, \mathbf{W}^2)$. In the following, we will omit the similar process in computing ϵ_g^1 , and instead focus on the treatment of teacher-average.

In analogous to ϵ_g^1 , the generalization error for task 2 can be expressed as

$$\epsilon_g^2 = \frac{1}{\pi} \arccos(p_2), \quad (\text{C31})$$

where $p_2 = \frac{1}{N} \sum_i \text{sign}(m_i) W_i^2$. Introducing p_2 to the replicated partition function results in a modified entropy term before taking the replica symmetry Ansatz,

$$\begin{aligned} (G'_S)^N &= \int_{\Omega^{nN}} \prod_{a=1}^n \prod_{i=1}^N dm_i^a e^{\sum_{a<b} \hat{q}_{ab} \sum_i m_i^a m_i^b + \frac{1}{2} \sum_a \hat{q}_{aa} \sum_i m_i^a m_i^a} \mathbb{E}_T \left[e^{\sum_a \hat{r}_a^1 \sum_i W_i^1 m_i^a + \sum_a \hat{p}_a^2 \sum_i W_i^2 \text{sign}(m_i^a)} \right] \\ &= \int_{\Omega^{nN}} \prod_{a=1}^n \prod_{i=1}^N dm_i^a e^{\sum_{a<b} \hat{q}_{ab} \sum_i m_i^a m_i^b + \frac{1}{2} \sum_a \hat{q}_{aa} \sum_i m_i^a m_i^a} \mathbb{E}_T \left[e^{\sum_a \hat{r}_a^1 \sum_i m_i^a + \sum_a \hat{p}_a^2 \sum_i W_i^1 W_i^2 \text{sign}(m_i^a)} \right], \end{aligned} \quad (\text{C32})$$

where the $\mathbb{E}_T[\cdot]$ denotes the teacher average. A gauge transformation $m_i^a \rightarrow m_i^a W_i^1$ is used in the second equality. Thus, the expectation can be computed as,

$$\begin{aligned} &\mathbb{E}_T \left[e^{\sum_a \hat{r}_a^1 \sum_i m_i^a + \sum_a \hat{p}_a^2 \sum_i W_i^1 W_i^2 \text{sign}(m_i^a)} \right] \\ &= \sum_{\mathbf{W}^1, \mathbf{W}^2} \prod_{i=1}^N P_0(W_i^1, W_i^2) e^{\sum_a \hat{r}_a^1 \sum_i m_i^a + \sum_a \hat{p}_a^2 \sum_i W_i^1 W_i^2 \text{sign}(m_i^a)} \\ &= \prod_{i=1}^N \sum_{W_i^1, W_i^2} P_0(W_i^1, W_i^2) e^{\sum_a \hat{r}_a^1 m_i^a + \sum_a \hat{p}_a^2 W_i^1 W_i^2 \text{sign}(m_i^a)} \\ &= \prod_{i=1}^N \left[\frac{1+r_0}{2} \cosh \left(\sum_a \hat{r}_a^1 m_i^a + \sum_a \hat{p}_a^2 \text{sign}(m_i^a) \right) + \frac{1-r_0}{2} \cosh \left(\sum_a \hat{r}_a^1 m_i^a - \sum_a \hat{p}_a^2 \text{sign}(m_i^a) \right) \right]. \end{aligned} \quad (\text{C33})$$

Under the replica symmetry Ansatz, we entropy term becomes,

$$G'_S = \int \mathcal{D}z \left[\left(\int_{-1}^{+1} dm e^{\frac{1}{2}\hat{q}_d m^2 - \frac{1}{2}\hat{q}_0 m^2 + \sqrt{\hat{q}_0} m z + \hat{r}_1 m + \hat{p}_2 \text{sign}(m)} \right)^n \frac{1+r_0}{2} + \left(\int_{-1}^{+1} dm e^{\frac{1}{2}\hat{q}_d m^2 - \frac{1}{2}\hat{q}_0 m^2 + \sqrt{\hat{q}_0} m z + \hat{r}_1 m - \hat{p}_2 \text{sign}(m)} \right)^n \frac{1-r_0}{2} \right]. \quad (\text{C34})$$

After taking the limitation of $n \rightarrow 0$, we have,

$$g'_S = \int \mathcal{D}z \ln \left(\int_{-1}^{+1} dm e^{\frac{1}{2}\hat{q}_d m^2 - \frac{1}{2}\hat{q}_0 m^2 + \sqrt{\hat{q}_0} m z + \hat{r}_1 m + \hat{p}_2 \text{sign}(m)} \right) \frac{1+r_0}{2} + \int \mathcal{D}z \ln \left(\int_{-1}^{+1} dm e^{\frac{1}{2}\hat{q}_d m^2 - \frac{1}{2}\hat{q}_0 m^2 + \sqrt{\hat{q}_0} m z + \hat{r}_1 m - \hat{p}_2 \text{sign}(m)} \right) \frac{1-r_0}{2}. \quad (\text{C35})$$

Therefore, we can finally get p_2 by $p_2 = \frac{\partial g'_S}{\partial \hat{p}_2}$, which results in

$$p_2 = r_0 \int \mathcal{D}z \langle \langle \text{sign}(m) \rangle \rangle_{\mathcal{I}(m,z)} = r_0 p_1, \quad (\text{C36})$$

which is actually linear to p_1 , and r_0 characterizes the task similarity.

c. Constrained partition function for learning process

The partition function Eq. (C3) defined previously focuses on the stationary state of the system, which helps to predict the optimal performance of learning given the corresponding Hamiltonian (loss function). However, by introducing a constraint in this system, we can study the stationary state during the learning process. The constrained partition function can be written as,

$$Z = \int_{\Omega} \prod_{i=1}^N dm_i \delta \left(\sum_i m_i^2 - q_{\star} N \right) e^{-\beta \mathcal{L}_1(\mathbf{m})}, \quad (\text{C37})$$

where $N - q_{\star} N$ is the total extent of the weight fluctuation. As the learning goes on, q_{\star} will gradually increase until a saturation to 1. Therefore, to explore the stationary state during learning, we can set a value of q_{\star} manually, and then solve the corresponding partition function Eq. (C37).

Note that, the calculation of the constrained partition function follows the similar procedure for the non-constrained one, except for one subtle difference, which is that the order

parameter q_{aa} as well as q_d under the replica symmetry Ansatz are replaced by a pre-specified constant q_* . Hence, we can directly derive the free energy density $-\beta f_{\text{RS}}$,

$$-\beta f_{\text{RS}} = \lim_{n \rightarrow 0} -\frac{1}{2} (\hat{q}_d q_* + (n-1)\hat{q}_0 q_0) - \hat{r}_1 r_1 + \frac{\ln G_S}{n} + \alpha_1 \frac{\ln G_E^*}{n}, \quad (\text{C38})$$

where the entropy term remains unchanged, and the energy term becomes

$$g_E^* = \lim_{n \rightarrow 0} \frac{\ln G_E^*}{n} = \int \mathcal{D}z \, 2H \left(-\frac{r_1}{\sqrt{q_0 - r_1^2}} z \right) \ln \int \mathcal{D}\sigma \, H^\beta \left(-\frac{\sqrt{q_* - q_0} \sigma + \sqrt{q_0} z}{\sqrt{1 - q_*}} \right). \quad (\text{C39})$$

Notice that q_* is a constant, and thus the saddle-point equations get simplified to

$$q_* = 2 \frac{\partial g_S}{\partial \hat{q}_d}, \quad q_0 = -2 \frac{\partial g_S}{\partial \hat{q}_0}, \quad r_1 = \frac{\partial g_S}{\partial \hat{r}_1}, \quad \hat{q}_0 = -2\alpha_1 \frac{\partial g_E^*}{\partial q_0}, \quad \hat{r}_1 = \alpha_1 \frac{\partial g_E^*}{\partial r_1}, \quad (\text{C40})$$

where the first one is an explicit equation for \hat{q}_d whose value can be numerically found (e.g., by using the secant method).

2. Thermodynamic system for multi-task learning

In the scenario of multi-task learning, a distinct characteristic is that previous task information is incorporated into the learning procedure of the current task by a regularization term. The task information from previous task refers to the trained weight for task 1, which can be captured by the associated partition function in the single-task learning section. In terms of the current task, a similar partition function should be established once the trained weights of the first task are given. This observation indicates that the variational continual learning *can be mapped* to the form of Franz-Parisi potential originally proposed in spin glass theory [23] and later in neural networks [22],

$$\Phi = \frac{1}{\tilde{Z}} \int_{\tilde{\Omega}} \prod_{i=1}^N d\tilde{m}_i \, e^{\tilde{\beta} \mathcal{L}_1(\tilde{\mathbf{m}})} \ln \int_{\Omega} \prod_{i=1}^N dm_i \, e^{\beta \mathcal{L}_2(\mathbf{m}, \tilde{\mathbf{m}})}, \quad (\text{C41})$$

where

$$\begin{aligned}\mathcal{L}_1(\tilde{\mathbf{m}}) &= \sum_{\mu=1}^{M_1} \ln H \left(-\frac{\text{sign}(\sum_i W_i^1 x_i^{1,\mu}) \sum_i m_i x_i^{1,\mu}}{\sqrt{\sum_i (1 - m_i^2)}} \right), \\ \mathcal{L}_2(\mathbf{m}, \tilde{\mathbf{m}}) &= \sum_{\mu=1}^{M_2} \ln H \left(-\frac{\text{sign}(\sum_i W_i^1 x_i^{2,\mu}) \sum_i m_i x_i^{2,\mu}}{\sqrt{\sum_i (1 - m_i^2)}} \right) - \sum_{i=1}^N \text{KL}(Q_{m_i} \| Q_{\tilde{m}_i}).\end{aligned}\tag{C42}$$

Next, our goal is to compute the quenched disorder average of the thermodynamic potential Φ , where the averages are threefold, consisting of two data averages over \mathcal{D}_1 and \mathcal{D}_2 , as well as the teacher average, and can be explicitly worked out as

$$\begin{aligned}\langle \Phi \rangle &= \mathbb{E}_{\mathbf{T}} \left\langle \frac{1}{\tilde{Z}} \int_{\tilde{\Omega}} \prod_{i=1}^N d\tilde{m}_i e^{\tilde{\beta} \mathcal{L}_1(\tilde{\mathbf{m}})} \ln \int_{\Omega} \prod_i^N dm_i e^{\beta \mathcal{L}_2(\mathbf{m}, \tilde{\mathbf{m}})} \right\rangle_{\mathcal{D}_1, \mathcal{D}_2} \\ &= \mathbb{E}_{\mathbf{T}} \frac{1}{\tilde{Z}} \int_{\tilde{\Omega}} \prod_{i=1}^N d\tilde{m}_i \prod_{\mu=1}^{M_1} \left\langle H^{\tilde{\beta}} \left(-\frac{\text{sign}(\sum_i W_i^1 x_i^{1,\mu}) \sum_i \tilde{m}_i x_i^{1,\mu}}{\sqrt{\sum_i (1 - \tilde{m}_i^2)}} \right) \right\rangle_{\mathcal{D}_1} \\ &\quad \ln \int_{\Omega} \prod_{i=1}^N dm_i \prod_{\mu=1}^{M_2} \left\langle H^{\beta} \left(-\frac{\text{sign}(\sum_i W_i^2 x_i^{2,\mu}) \sum_i m_i x_i^{2,\mu}}{\sqrt{\sum_i (1 - m_i^2)}} \right) \right\rangle_{\mathcal{D}_2} e^{-\beta \sum_i \text{KL}(m_i, \tilde{m}_i)}.\end{aligned}\tag{C43}$$

Note that two data averages decouple directly due to the independence between two datasets (but the labels can be correlated). We now omit the subscripts for the data averages. To start the calculation, we introduce two useful replica formulas, $\frac{1}{\tilde{Z}} = \lim_{n \rightarrow 0} \tilde{Z}^{n-1}$, $\ln Z = \lim_{s \rightarrow 0} \partial_s Z^s$. Then the potential turns out to be

$$\begin{aligned}\langle \Phi \rangle &= \lim_{n \rightarrow 0} \lim_{s \rightarrow 0} \partial_s \mathbb{E}_{\mathbf{T}} \int_{\tilde{\Omega}^{nN}} \prod_{a=1}^n \prod_{i=1}^N d\tilde{m}_i^a \prod_{a=1}^n \prod_{\mu=1}^{M_1} \left\langle H^{\tilde{\beta}} \left(-\frac{\text{sign}(\sum_i W_i^1 x_i^{1,\mu}) \sum_i \tilde{m}_i^a x_i^{1,\mu}}{\sqrt{\sum_i (1 - (\tilde{m}_i^a)^2)}} \right) \right\rangle \\ &\quad \int_{\Omega^{sN}} \prod_{c=1}^s \prod_{i=1}^N dm_i^c \prod_{c=1}^s \prod_{\mu=1}^{M_2} \left\langle H^{\beta} \left(-\frac{\text{sign}(\sum_i W_i^2 x_i^{2,\mu}) \sum_i m_i^c x_i^{2,\mu}}{\sqrt{\sum_i (1 - (m_i^c)^2)}} \right) \right\rangle e^{-\beta \sum_c \sum_i \text{KL}(m_i^c, \tilde{m}_i^a=1)}.\end{aligned}\tag{C44}$$

Local fields are introduced for both loss functions,

$$\tilde{u}^a = \frac{\sum_i \tilde{m}_i^a x_i^1}{\sqrt{N}}, \quad \tilde{v}_1 = \frac{\sum_i W_i^1 x_i^1}{\sqrt{N}}, \quad u^c = \frac{\sum_i m_i^c x_i^2}{\sqrt{N}}, \quad v_2 = \frac{\sum_i W_i^2 x_i^2}{\sqrt{N}},\tag{C45}$$

where we omit superscript μ . Based on the central limit theorem, the local fields follow the

joint Gaussian distribution with zero mean and the non-zero second moments as,

$$\begin{aligned}\langle \tilde{u}^a \tilde{u}^a \rangle &= \frac{\sum_i \tilde{m}_i^a \tilde{m}_i^a}{N}, & \langle \tilde{u}^a \tilde{u}^b \rangle &= \frac{\sum_i \tilde{m}_i^a \tilde{m}_i^b}{N}, & \langle \tilde{v}_1 \tilde{u}^a \rangle &= \frac{\sum_i W_i^1 \tilde{m}_i^a}{N}, & \langle \tilde{v}_1 \tilde{v}_1 \rangle &= 1, \\ \langle u^c u^c \rangle &= \frac{\sum_i m_i^c m_i^c}{N}, & \langle u^c u^d \rangle &= \frac{\sum_i m_i^c m_i^d}{N}, & \langle v_2 u^c \rangle &= \frac{\sum_i W_i^2 m_i^c}{N}, & \langle v_2 v_2 \rangle &= 1.\end{aligned}\tag{C46}$$

We can therefore define the order parameters, $\tilde{q}_{aa} = \frac{\sum_i \tilde{m}_i^a \tilde{m}_i^a}{N}$, $\tilde{q}_{ab} = \frac{\sum_i \tilde{m}_i^a \tilde{m}_i^b}{N}$, $\tilde{r}_a^1 = \frac{\sum_i W_i^1 \tilde{m}_i^a}{N}$, $q_{cc} = \frac{\sum_i m_i^c m_i^c}{N}$, $q_{cd} = \frac{\sum_i m_i^c m_i^d}{N}$, $r_c^2 = \frac{\sum_i W_i^2 m_i^c}{N}$ and enforce these definitions in potential Φ by Dirac delta function $\delta(\cdot)$. After a few algebra manipulations, we arrive at

$$\langle \Phi \rangle = \lim_{n \rightarrow 0} \lim_{s \rightarrow 0} \partial_s \int \prod_a \frac{d\hat{q}_{aa} d\tilde{q}_{aa}}{4\pi i/N} \prod_{a < b} \frac{d\hat{q}_{ab} d\tilde{q}_{ab}}{2\pi i/N} \prod_a \frac{d\hat{r}_a^1 d\tilde{r}_a^1}{2\pi i/N} \prod_c \frac{d\hat{q}_{cc} dq_{cc}}{4\pi i/N} \prod_{c < d} \frac{d\hat{q}_{cd} dq_{cd}}{2\pi i/N} \prod_c \frac{d\hat{r}_c^2 dr_c^2}{2\pi i/N} e^{NS},\tag{C47}$$

where a similar manipulation of the teacher average to Eq. (C33) is carried out, and the action \mathcal{S} finally reads

$$\begin{aligned}\mathcal{S} &= -\frac{1}{2} \sum_{a,b} \hat{q}_{ab} \tilde{q}_{ab} - \sum_a \hat{r}_a^1 \tilde{r}_a^1 - \frac{1}{2} \sum_{c,d} \hat{q}_{cd} q_{cd} - \sum_c \hat{r}_c^2 r_c^2 \\ &+ \ln \int_{\hat{\Omega}^{nN}} \int_{\Omega^{sN}} \prod_a d\tilde{m}_a \prod_c dm_c e^{\frac{1}{2} \sum_{a,b} \hat{q}_{ab} \tilde{m}_a \tilde{m}_b + \frac{1}{2} \sum_{c,d} \hat{q}_{cd} m_c m_d - \beta \sum_c \text{KL}(m_c^c; \tilde{m}_i^{a=1})} \\ &\times \left[\frac{1+r_0}{2} \cosh \left(\sum_a \hat{r}_a^1 \tilde{m}_i^a + \sum_c \hat{r}_c^2 m_i^c \right) + \frac{1-r_0}{2} \cosh \left(\sum_a \hat{r}_a^1 \tilde{m}_i^a - \sum_c \hat{r}_c^2 m_i^c \right) \right] \\ &+ \alpha_1 \ln \left\langle \prod_{a=1}^n H^{\tilde{\beta}} \left(-\frac{\text{sign}(\tilde{v}_1) \tilde{u}^a}{\sqrt{1-\tilde{q}_{aa}}} \right) \right\rangle + \alpha_2 \ln \left\langle \prod_{c=1}^s H^{\beta} \left(-\frac{\text{sign}(v_2) u^c}{\sqrt{1-q_{cc}}} \right) \right\rangle.\end{aligned}\tag{C48}$$

The maximum of \mathcal{S} dominates the integrand under the large N limit. Thus, we derive the saddle-point equations by taking derivatives of the action \mathcal{S} with respect to the order parameters. We then apply the replica symmetry Ansatz,

$$\begin{aligned}\tilde{q}_{ab} &= \tilde{q}_0, & \hat{q}_{ab} &= \hat{q}_0, & \tilde{q}_{aa} &= \tilde{q}_d, & \hat{q}_{aa} &= \hat{q}_d, & \tilde{r}_a^1 &= \tilde{r}_1, & \hat{r}_a^1 &= \hat{r}_1, \\ q_{cd} &= q_0, & \hat{q}_{cd} &= \hat{q}_0, & q_{cc} &= q_d, & \hat{q}_{cc} &= \hat{q}_d, & r_c^2 &= r_2, & \hat{r}_c^2 &= \hat{r}_2.\end{aligned}\tag{C49}$$

To make the calculation neat, we divide the action into three parts and compute their

contributions respectively. First, the interaction term reads

$$\begin{aligned}
\mathcal{G}_I &= -\frac{1}{2} \sum_{a,b} \hat{q}_{ab} \tilde{q}_{ab} - \sum_a \hat{r}_a^1 \tilde{r}_a^1 - \frac{1}{2} \sum_{c,d} \hat{q}_{cd} q_{cd} - \sum_c \hat{r}_c^2 r_c^2 \\
&= -\frac{1}{2} \left(\sum_a \hat{q}_{aa} \tilde{q}_{aa} + \sum_{a \neq b} \hat{q}_{ab} \tilde{q}_{ab} \right) - \frac{1}{2} \left(\sum_c \hat{q}_{cc} q_{cc} + \sum_{c \neq d} \hat{q}_{cd} q_{cd} \right) - n \hat{r}_1 \tilde{r}_1 - s \hat{r}_2 r_2 \quad (\text{C50}) \\
&= -\frac{1}{2} \left(n \hat{q}_d \tilde{q}_d + s(s-1) \hat{q}_0 q_0 \right) - \frac{1}{2} \left(s \hat{q}_d q_d + n(n-1) \hat{q}_0 q_0 \right) - n \hat{r}_1 \tilde{r}_1 - s \hat{r}_2 r_2.
\end{aligned}$$

Then, the entropy term can be given by

$$\begin{aligned}
\mathcal{G}_S &= \int_{\tilde{\Omega}^{nN}} \int_{\Omega^{sN}} \prod_a d\tilde{m}_a \prod_c dm_c e^{\frac{1}{2} \sum_{a,b} \hat{q}_{ab} \tilde{m}_a \tilde{m}_b + \frac{1}{2} \sum_{c,d} \hat{q}_{cd} m_c m_d - \beta \sum_c \text{KL}(m_i^c, \tilde{m}_i^{a=1})} \\
&\quad \times \left[\frac{1+r_0}{2} \cosh \left(\sum_a \hat{r}_a^1 \tilde{m}_i^a + \sum_c \hat{r}_c^2 m_i^c \right) + \frac{1-r_0}{2} \cosh \left(\sum_a \hat{r}_a^1 \tilde{m}_i^a - \sum_c \hat{r}_c^2 m_i^c \right) \right] \\
&= \int_{\tilde{\Omega}^{nN}} \int_{\Omega^{sN}} \prod_a d\tilde{m}_a \prod_c dm_c \int \mathcal{D}z_1 \int \mathcal{D}z_2 e^{\frac{1}{2}(\hat{q}_d - \hat{q}_0) \sum_a (\tilde{m}_a)^2 + \sqrt{\hat{q}_0} z_1 \sum_a \tilde{m}_a + \frac{1}{2}(\hat{q}_d - \hat{q}_0) \sum_c (m_c)^2 + \sqrt{\hat{q}_0} z_2 \sum_c m_c} \\
&\quad e^{-\beta \sum_c \text{KL}(m_i^c, \tilde{m}_i^{a=1})} \left[\frac{1+r_0}{2} \cosh \left(\sum_a \hat{r}_a^1 \tilde{m}_i^a + \sum_c \hat{r}_c^2 m_i^c \right) + \frac{1-r_0}{2} \cosh \left(\sum_a \hat{r}_a^1 \tilde{m}_i^a - \sum_c \hat{r}_c^2 m_i^c \right) \right] \\
&= \frac{1+r_0}{2} \int \mathcal{D}z_1 \left(\int_{-1}^{+1} d\tilde{m} e^{\tilde{\mathcal{I}}(\tilde{m}, z_1)} \right)^{n-1} \int_{-1}^{+1} d\tilde{m} e^{\tilde{\mathcal{I}}(\tilde{m}, z_1)} \int \mathcal{D}z_2 \left(\int_{-1}^{+1} dm e^{\mathcal{J}^+(m, \tilde{m}, z_2)} \right)^s \\
&\quad + \frac{1-r_0}{2} \int \mathcal{D}z_1 \left(\int_{-1}^{+1} d\tilde{m} e^{\tilde{\mathcal{I}}(\tilde{m}, z_1)} \right)^{n-1} \int_{-1}^{+1} d\tilde{m} e^{\tilde{\mathcal{I}}(\tilde{m}, z_1)} \int \mathcal{D}z_2 \left(\int_{-1}^{+1} dm e^{\mathcal{J}^-(m, \tilde{m}, z_2)} \right)^s, \quad (\text{C51})
\end{aligned}$$

where

$$\begin{aligned}
\tilde{\mathcal{I}}(\tilde{m}, z_1) &= \frac{1}{2}(\hat{q}_d - \hat{q}_0) \tilde{m}^2 + \left(\hat{r}_1 + \sqrt{\hat{q}_0} z_1 \right) \tilde{m}, \\
\mathcal{J}^+(m, \tilde{m}, z_2) &= \frac{1}{2}(\hat{q}_d - \hat{q}_0) m^2 + \left(\hat{r}_2 + \sqrt{\hat{q}_0} z_2 \right) m - \beta \text{KL}(m, \tilde{m}), \\
\mathcal{J}^-(m, \tilde{m}, z_2) &= \frac{1}{2}(\hat{q}_d - \hat{q}_0) m^2 + \left(\hat{r}_2 + \sqrt{\hat{q}_0} z_2 \right) m - \beta \text{KL}(m, -\tilde{m}), \quad (\text{C52}) \\
\text{KL}(x, y) &= - \sum_{z=\pm 1} \left[\mathcal{K}\left(\frac{1+xz}{2}, \frac{1+yz}{2}\right) - \mathcal{K}\left(\frac{1+xz}{2}, \frac{1+xz}{2}\right) \right],
\end{aligned}$$

where $\mathcal{K}(x, y) = x \ln y$. Finally, we derive the energy term, expressed as

$$\begin{aligned} \mathcal{G}_E^1 &= \left\langle \prod_{a=1}^n H^{\tilde{\beta}} \left(-\frac{\text{sign}(\tilde{v}_1) \tilde{u}^a}{\sqrt{1 - \tilde{q}_{aa}}} \right) \right\rangle \\ &= \int \mathcal{D}z \, 2H \left(-\frac{\tilde{r}_1}{\sqrt{\tilde{q}_0 - \tilde{r}_1^2}} z \right) \left(\int \mathcal{D}\sigma \, H^{\tilde{\beta}} \left(-\frac{\sqrt{\tilde{q}_d - \tilde{q}_0 \sigma} + \sqrt{\tilde{q}_0} z}{\sqrt{1 - \tilde{q}_d}} \right) \right)^n, \end{aligned} \quad (\text{C53})$$

and

$$\begin{aligned} \mathcal{G}_E^2 &= \left\langle \prod_{c=1}^s H^\beta \left(-\frac{\text{sign}(v_2) u^c}{\sqrt{1 - q_{cc}}} \right) \right\rangle \\ &= \int \mathcal{D}z \, 2H \left(-\frac{r_2}{\sqrt{q_0 - r_2^2}} z \right) \left(\int \mathcal{D}\sigma \, H^\beta \left(-\frac{\sqrt{q_d - q_0 \sigma} + \sqrt{q_0} z}{\sqrt{1 - q_d}} \right) \right)^s, \end{aligned} \quad (\text{C54})$$

where we follow the same computation as deriving Eq. (C14). Thus, we summarize the result as

$$\mathcal{S} = -\frac{1}{2} \left(n \hat{q}_d \tilde{q}_d + s(s-1) \hat{q}_0 q_0 \right) - \frac{1}{2} \left(s \hat{q}_d q_d + n(n-1) \hat{q}_0 q_0 - n \hat{r}_1 \tilde{r}_1 - s \hat{r}_2 r_2 + \ln \mathcal{G}_S + \alpha_1 \ln \mathcal{G}_E^1 + \alpha_2 \ln \mathcal{G}_E^2 \right). \quad (\text{C55})$$

Calculation of saddle-point equations requires to consider the limits of $\lim_{n \rightarrow 0}$ and $\lim_{s \rightarrow 0}$, which leads to the computation of $\lim_{n \rightarrow 0} \lim_{s \rightarrow 0} \frac{\ln \mathcal{G}_S}{n}$, $\lim_{n \rightarrow 0} \lim_{s \rightarrow 0} \frac{\ln \mathcal{G}_S}{s}$, $\lim_{n \rightarrow 0} \lim_{s \rightarrow 0} \frac{\ln \mathcal{G}_E^1}{n}$,

and $\lim_{n \rightarrow 0} \lim_{s \rightarrow 0} \frac{\ln \mathcal{G}_E^2}{s}$. Thus, we define and compute these quantities first.

$$\begin{aligned}
\tilde{g}_S &= \lim_{n \rightarrow 0} \lim_{s \rightarrow 0} \frac{\ln \mathcal{G}_S}{n} \\
&= \int \mathcal{D}z \ln \int_{-1}^{+1} d\tilde{m} e^{\tilde{\mathcal{I}}(\tilde{m}, z)}, \\
g_S &= \lim_{n \rightarrow 0} \lim_{s \rightarrow 0} \frac{\ln \mathcal{G}_S}{s} \\
&= \frac{1+r_0}{2} \int \mathcal{D}z_1 \left\langle \left\langle \int \mathcal{D}z_2 \ln \int_{-1}^{+1} e^{\mathcal{J}^+(m, \tilde{m}, z_2)} \right\rangle \right\rangle_{\tilde{\mathcal{I}}(\tilde{m}, z_1)} \\
&\quad + \frac{1-r_0}{2} \int \mathcal{D}z_1 \left\langle \left\langle \int \mathcal{D}z_2 \ln \int_{-1}^{+1} e^{\mathcal{J}^-(m, \tilde{m}, z_2)} \right\rangle \right\rangle_{\tilde{\mathcal{I}}(\tilde{m}, z_1)}, \tag{C56} \\
\tilde{g}_E &= \lim_{n \rightarrow 0} \lim_{s \rightarrow 0} \frac{\ln \mathcal{G}_E^1}{n} \\
&= \int \mathcal{D}z \, 2H \left(-\frac{\tilde{r}_1}{\sqrt{\tilde{q}_0 - \tilde{r}_1^2}} z \right) \ln \int \mathcal{D}\sigma \, H^\beta \left(-\frac{\sqrt{\tilde{q}_d - \tilde{q}_0} \sigma + \sqrt{\tilde{q}_0} z}{\sqrt{1 - \tilde{q}_d}} \right), \\
g_E &= \lim_{n \rightarrow 0} \lim_{s \rightarrow 0} \frac{\ln \mathcal{G}_E^2}{s} \\
&= \int \mathcal{D}z \, 2H \left(-\frac{r_2}{\sqrt{q_0 - r_2^2}} z \right) \ln \int \mathcal{D}\sigma \, H^\beta \left(-\frac{\sqrt{q_d - q_0} \sigma + \sqrt{q_0} z}{\sqrt{1 - q_d}} \right).
\end{aligned}$$

Then, we can arrive at the saddle-point equations given below.

$$\begin{aligned}
\tilde{q}_d &= 2 \frac{\partial \tilde{g}_S}{\partial \hat{q}_d}, & \tilde{q}_0 &= -2 \frac{\partial \tilde{g}_S}{\partial \hat{q}_0}, & \tilde{r}_1 &= \frac{\partial \tilde{g}_S}{\partial \hat{r}_1}, & \hat{q}_d &= 2\alpha_1 \frac{\partial \tilde{g}_E}{\partial \hat{q}_d}, & \hat{q}_0 &= -2\alpha_1 \frac{\partial \tilde{g}_E}{\partial \hat{q}_0}, & \hat{r}_1 &= \alpha_1 \frac{\partial \tilde{g}_E}{\partial \hat{r}_1}; \\
q_d &= 2 \frac{\partial g_S}{\partial \hat{q}_d}, & q_0 &= -2 \frac{\partial g_S}{\partial \hat{q}_0}, & r_2 &= \frac{\partial g_S}{\partial \hat{r}_2}, & \hat{q}_d &= 2\alpha_2 \frac{\partial g_E}{\partial \hat{q}_d}, & \hat{q}_0 &= -2\alpha_2 \frac{\partial g_E}{\partial \hat{q}_0}, & \hat{r}_2 &= \alpha_2 \frac{\partial g_E}{\partial \hat{r}_2}. \tag{C57}
\end{aligned}$$

It is easy to verify that the tilde order parameters are exactly the same as those in Eq. (C18), which are independent of the non-tilde order parameters. This is reasonable because in the multi-task loss function $\mathcal{L}_2(\mathbf{m}, \tilde{\mathbf{m}})$, the magnetization $\tilde{\mathbf{m}}$ in the KL-divergence is the solution after learning the first task, which is described by the single-task partition function Eq. (C3). As for the non-tilde order parameters, the hatted ones are in the same form with Eqs. (C22,C23), except for the replacement of r_1 by r_2 in Eq. (C23). After a few

manipulations, the second-task related order parameters are expressed as follows,

$$\begin{aligned}
q_d &= \frac{1+r_0}{2} \int \mathcal{D}z_1 \left\langle \left\langle \int \mathcal{D}z_2 \langle \langle m^2 \rangle \rangle_{\mathcal{J}^+(m, \tilde{m}, z_2)} \right\rangle \right\rangle_{\tilde{\mathcal{I}}(\tilde{m}, z_1)} \\
&\quad + \frac{1-r_0}{2} \int \mathcal{D}z_1 \left\langle \left\langle \int \mathcal{D}z_2 \langle \langle m^2 \rangle \rangle_{\mathcal{J}^-(m, \tilde{m}, z_2)} \right\rangle \right\rangle_{\tilde{\mathcal{I}}(\tilde{m}, z_1)}, \\
q_0 &= \frac{1+r_0}{2} \int \mathcal{D}z_1 \left\langle \left\langle \int \mathcal{D}z_2 \left\langle \left\langle m^2 - \frac{z}{\sqrt{q_0}} m \right\rangle \right\rangle_{\mathcal{J}^+(m, \tilde{m}, z_2)} \right\rangle \right\rangle_{\tilde{\mathcal{I}}(\tilde{m}, z_1)} \\
&\quad + \frac{1-r_0}{2} \int \mathcal{D}z_1 \left\langle \left\langle \int \mathcal{D}z_2 \left\langle \left\langle m^2 - \frac{z}{\sqrt{q_0}} m \right\rangle \right\rangle_{\mathcal{J}^-(m, \tilde{m}, z_2)} \right\rangle \right\rangle_{\tilde{\mathcal{I}}(\tilde{m}, z_1)}, \\
r_2 &= \frac{1+r_0}{2} \int \mathcal{D}z_1 \left\langle \left\langle \int \mathcal{D}z_2 \langle \langle m \rangle \rangle_{\mathcal{J}^+(m, \tilde{m}, z_2)} \right\rangle \right\rangle_{\tilde{\mathcal{I}}(\tilde{m}, z_1)} \\
&\quad + \frac{1-r_0}{2} \int \mathcal{D}z_1 \left\langle \left\langle \int \mathcal{D}z_2 \langle \langle m \rangle \rangle_{\mathcal{J}^-(m, \tilde{m}, z_2)} \right\rangle \right\rangle_{\tilde{\mathcal{I}}(\tilde{m}, z_1)}.
\end{aligned} \tag{C58}$$

a. Generalization error for two tasks

The derivation of generalization error in the multi-task scenario follows the same procedure with the single-task scenario. Thus, we present the final results directly. After the convergence of all order parameters, the generalization error for task 2 reads

$$\epsilon_g^2 = \frac{1}{\pi} \arccos(p_2), \tag{C59}$$

where

$$\begin{aligned}
p_2 &= \frac{1+r_0}{2} \int \mathcal{D}z_1 \left\langle \left\langle \int \mathcal{D}z_2 \langle \langle \text{sign}(m) \rangle \rangle_{\mathcal{J}^+(m, \tilde{m}, z_2)} \right\rangle \right\rangle_{\tilde{\mathcal{I}}(\tilde{m}, z_1)} \\
&\quad + \frac{1-r_0}{2} \int \mathcal{D}z_1 \left\langle \left\langle \int \mathcal{D}z_2 \langle \langle \text{sign}(m) \rangle \rangle_{\mathcal{J}^-(m, \tilde{m}, z_2)} \right\rangle \right\rangle_{\tilde{\mathcal{I}}(\tilde{m}, z_1)}.
\end{aligned} \tag{C60}$$

The generalization error for task 1 reads

$$\epsilon_g^1 = \frac{1}{\pi} \arccos(p_1), \tag{C61}$$

where

$$p_1 = \frac{1+r_0}{2} \int \mathcal{D}z_1 \left\langle \left\langle \int \mathcal{D}z_2 \langle \langle \text{sign}(m) \rangle \rangle_{\mathcal{J}^+(m, \tilde{m}, z_2)} \right\rangle \right\rangle_{\tilde{\mathcal{I}}(\tilde{m}, z_1)} - \frac{1-r_0}{2} \int \mathcal{D}z_1 \left\langle \left\langle \int \mathcal{D}z_2 \langle \langle \text{sign}(m) \rangle \rangle_{\mathcal{J}^-(m, \tilde{m}, z_2)} \right\rangle \right\rangle_{\tilde{\mathcal{I}}(\tilde{m}, z_1)}. \quad (\text{C62})$$

b. The case of tunned KL terms

To investigate the regularization term, we can multiply this term with a factor γ , and then derive the saddle point equations for the multi-task learning as above. Finally we can change the value of the modulation factor to probe effects of the regularization term. The objective function then reads

$$\mathcal{L}_2(\mathbf{m}, \tilde{\mathbf{m}}, \gamma) = \sum_{\mu=1}^{M_2} \ln H \left(-\frac{\text{sign}(\sum_i W_i^1 x_i^{2,\mu}) \sum_i m_i x_i^{2,\mu}}{\sqrt{\sum_i (1-m_i^2)}} \right) - \gamma \sum_{i=1}^N \text{KL}(Q_{m_i} | Q_{m_i^1}). \quad (\text{C63})$$

This minor change will not affect the whole calculation process, but only induce a corresponding factor in the auxiliary terms,

$$\begin{aligned} \mathcal{J}^+(m, \tilde{m}, z_2, \gamma) &= \frac{1}{2}(\hat{q}_d - \hat{q}_0)m^2 + \left(\hat{r}_2 + \sqrt{\hat{q}_0}z_2 \right) m - \gamma\beta\text{KL}(m, \tilde{m}), \\ \mathcal{J}^-(m, \tilde{m}, z_2, \gamma) &= \frac{1}{2}(\hat{q}_d - \hat{q}_0)m^2 + \left(\hat{r}_2 + \sqrt{\hat{q}_0}z_2 \right) m - \gamma\beta\text{KL}(m, -\tilde{m}). \end{aligned} \quad (\text{C64})$$

Thus, the saddle-points equations remain the same except for the following differences,

$$\begin{aligned} q_d &= \frac{1+r_0}{2} \int \mathcal{D}z_1 \left\langle \left\langle \int \mathcal{D}z_2 \langle \langle m^2 \rangle \rangle_{\mathcal{J}^+(m, \tilde{m}, z_2, \gamma)} \right\rangle \right\rangle_{\tilde{\mathcal{I}}(\tilde{m}, z_1)} \\ &\quad + \frac{1-r_0}{2} \int \mathcal{D}z_1 \left\langle \left\langle \int \mathcal{D}z_2 \langle \langle m^2 \rangle \rangle_{\mathcal{J}^-(m, \tilde{m}, z_2, \gamma)} \right\rangle \right\rangle_{\tilde{\mathcal{I}}(\tilde{m}, z_1)}, \\ q_0 &= \frac{1+r_0}{2} \int \mathcal{D}z_1 \left\langle \left\langle \int \mathcal{D}z_2 \left\langle \left\langle m^2 - \frac{z}{\sqrt{q_0}}m \right\rangle \right\rangle_{\mathcal{J}^+(m, \tilde{m}, z_2, \gamma)} \right\rangle \right\rangle_{\tilde{\mathcal{I}}(\tilde{m}, z_1)} \\ &\quad + \frac{1-r_0}{2} \int \mathcal{D}z_1 \left\langle \left\langle \int \mathcal{D}z_2 \left\langle \left\langle m^2 - \frac{z}{\sqrt{q_0}}m \right\rangle \right\rangle_{\mathcal{J}^-(m, \tilde{m}, z_2, \gamma)} \right\rangle \right\rangle_{\tilde{\mathcal{I}}(\tilde{m}, z_1)}, \\ r_2 &= \frac{1+r_0}{2} \int \mathcal{D}z_1 \left\langle \left\langle \int \mathcal{D}z_2 \langle \langle m \rangle \rangle_{\mathcal{J}^+(m, \tilde{m}, z_2, \gamma)} \right\rangle \right\rangle_{\tilde{\mathcal{I}}(\tilde{m}, z_1)} \\ &\quad + \frac{1-r_0}{2} \int \mathcal{D}z_1 \left\langle \left\langle \int \mathcal{D}z_2 \langle \langle m \rangle \rangle_{\mathcal{J}^-(m, \tilde{m}, z_2, \gamma)} \right\rangle \right\rangle_{\tilde{\mathcal{I}}(\tilde{m}, z_1)}. \end{aligned} \quad (\text{C65})$$

Acknowledgments

We thank the referee for many constructive comments to improve the quality of the paper. This research was supported by the National Key R&D Program of China (2019YFA0706302) and the National Natural Science Foundation of China for Grant Number 12122515 (H.H.), and the National Natural Science Foundation of China for Grant Number 11975295 (Z.H.), and Guangdong Provincial Key Laboratory of Magnetoelectric Physics and Devices (No. 2022B1212010008), and Guangdong Basic and Applied Basic Research Foundation (Grant No. 2023B1515040023).

-
- [1] Michael McCloskey and Neal J. Cohen. Catastrophic interference in connectionist networks: The sequential learning problem. *Psychology of Learning and Motivation*, 24:109–165, 1989.
 - [2] German I. Parisi, Ronald Kemker, Jose L. Part, Christopher Kanan, and Stefan Wermter. Continual lifelong learning with neural networks: A review. *Neural Networks*, 113:54–71, 2019.
 - [3] Salomon Z. Muller, Abigail N. Zadina, L.F. Abbott, and Nathaniel B. Sawtell. Continual learning in a multi-layer network of an electric fish. *Cell*, 179(6):1382–1392.e10, 2019.
 - [4] Yang Shen, Sanjoy Dasgupta, and Saket Navlakha. Algorithmic insights on continual learning from fruit flies. *arXiv:2107.07617*, 2021.
 - [5] Timo Flesch, Andrew M. Saxe, and Christopher Summerfield. Continual task learning in natural and artificial agents. *arXiv:2210.04520*, 2022.
 - [6] Nicolas Y. Masse, Gregory D. Grant, and David J. Freedman. Alleviating catastrophic forgetting using context-dependent gating and synaptic stabilization. *Proceedings of the National Academy of Sciences*, 115(44):E10467–E10475, 2018.
 - [7] Gido M. van de Ven, Hava T. Siegelmann, and Andreas S. Tolias. Brain-inspired replay for continual learning with artificial neural networks. *Nature Communications*, 11(1):4069, 2020.
 - [8] Axel Laborieux, Maxence Ernout, Tifenn Hirtzlin, and Damien Querlioz. Synaptic metaplasticity in binarized neural networks. *Nature Communications*, 12(1):2549, 2021.
 - [9] James Kirkpatrick, Razvan Pascanu, Neil Rabinowitz, Joel Veness, Guillaume Desjardins, Andrei A. Rusu, Kieran Milan, John Quan, Tiago Ramalho, Agnieszka Grabska-Barwinska,

- Demis Hassabis, Claudia Clopath, Dharshan Kumaran, and Raia Hadsell. Overcoming catastrophic forgetting in neural networks. *Proceedings of the National Academy of Sciences*, 114(13):3521–3526, 2017.
- [10] Friedemann Zenke, Ben Poole, and Surya Ganguli. Continual learning through synaptic intelligence. *Proceedings of machine learning research*, 70:3987–3995, 2017.
- [11] Joan Serra, Didac Suris, Marius Miron, and Alexandros Karatzoglou. Overcoming catastrophic forgetting with hard attention to the task. In Jennifer Dy and Andreas Krause, editors, *Proceedings of the 35th International Conference on Machine Learning*, volume 80 of *Proceedings of Machine Learning Research*, pages 4548–4557. PMLR, 2018.
- [12] Sebastian Farquhar and Yarin Gal. A unifying bayesian view of continual learning. *arXiv:1902.06494*, 2019.
- [13] Chen Zeno, Itay Golan, Elad Hoffer, and Daniel Soudry. Task agnostic continual learning using online variational bayes. *arXiv:1803.10123*, 2018.
- [14] Cuong V. Nguyen, Yingzhen Li, Thang D. Bui, and Richard E. Turner. Variational continual learning. In *International Conference on Learning Representations*, 2018.
- [15] Sayna Ebrahimi, Mohamed Elhoseiny, Trevor Darrell, and Marcus Rohrbach. Uncertainty-guided continual learning with bayesian neural networks. In *International Conference on Learning Representations*, 2020.
- [16] Tameem Adel, Han Zhao, and Richard E. Turner. Continual learning with adaptive weights (claw). In *International Conference on Learning Representations*, 2020.
- [17] Oussama Dhifallah and Yue M. Lu. Phase transitions in transfer learning for high-dimensional perceptrons. *Entropy*, 23:400, 2021.
- [18] Anthony Ndirango and Tyler Lee. Generalization in multitask deep neural classifiers: a statistical physics approach. In H. Wallach, H. Larochelle, A. Beygelzimer, F. d Alche-Buc, E. Fox, and R. Garnett, editors, *Advances in Neural Information Processing Systems*, volume 32. Curran Associates, Inc., 2019.
- [19] Haruka Asanuma, Shiro Takagi, Yoshihiro Nagano, Yuki Yoshida, Yasuhiko Igarashi, and Masato Okada. Statistical mechanical analysis of catastrophic forgetting in continual learning with teacher and student networks. *Journal of the Physical Society of Japan*, 90(10):104001, 2021.
- [20] Sebastian Lee, Sebastian Goldt, and Andrew Saxe. Continual learning in the teacher-student

- setup: Impact of task similarity. *arXiv:2107.04384*, 2021.
- [21] Alexandre Pouget, Jeffrey M Beck, Wei Ji Ma, and Peter E Latham. Probabilistic brains: knowns and unknowns. *Nature Neuroscience*, 16(9):1170–1178, 2013.
- [22] Haiping Huang and Yoshiyuki Kabashima. Origin of the computational hardness for learning with binary synapses. *Physical review. E*, 90:052813, 2014.
- [23] Silvio Franz and Giorgio Parisi. Recipes for metastable states in spin glasses. *Journal De Physique I*, 5(11):1401–1415, 1995.
- [24] Haiping Huang. *Statistical Mechanics of Neural Networks*. Springer, Singapore, 2022.
- [25] W. Krauth and M. Mézard. Storage capacity of memory networks with binary couplings. *J. Phys. (France)*, 50:3057, 1989.
- [26] G Gyorgyi. First-order transition to perfect generalization in a neural network with binary synapses. *Physical Review A*, 41(12):7097–7100, 1990.
- [27] H. Sompolinsky, N. Tishby, and Hyunjune Sebastian Seung. Learning from examples in large neural networks. *Physical review letters*, 65:1683–1686, 1990.
- [28] Chan Li and Haiping Huang. Learning credit assignment. *Phys. Rev. Lett.*, 125:178301, 2020.
- [29] Carlo Baldassi, Federica Gerace, Hilbert J. Kappen, Carlo Lucibello, Luca Saglietti, Enzo Tartaglione, and Riccardo Zecchina. Role of synaptic stochasticity in training low-precision neural networks. *Phys. Rev. Lett.*, 120:268103, 2018.
- [30] Haiping Huang. Variational mean-field theory for training restricted boltzmann machines with binary synapses. *Phys. Rev. E*, 102:030301(R), 2020.
- [31] Laurence Aitchison, Jannes Jegminat, Jorge Aurelio Menendez, Jean-Pascal Pfister, Alexandre Pouget, and Peter E. Latham. Synaptic plasticity as bayesian inference. *Nature neuroscience*, 24:565–571, 2021.
- [32] <https://github.com/Chan-Li/VCL>.